Faddeev calculation of 3α and $\alpha\alpha\Lambda$ systems using $\alpha\alpha$ resonating-group method kernels

Y. Fujiwara,[1,*] K. Miyagawa,[2] M. Kohno,[3] Y. Suzuki,[4] D. Baye,[5] and J.-M. Sparenberg[5,6]
[1]*Department of Physics, Kyoto University, Kyoto 606-8502, Japan*
[2]*Department of Applied Physics, Okayama Science University, Okayama 700-0005, Japan*
[3]*Physics Division, Kyushu Dental College, Kitakyushu 803-8580, Japan*
[4]*Department of Physics, Niigata University, Niigata 950-2181, Japan*
[5]*Physique Nucléaire Théorique et Physique Mathématique, CP 229, Université Libre de Bruxelles, B-1050 Brussels, Belgium*
[6]*TRIUMF, 4004 Wesbrook Mall, Vancouver, British Columbia, Canada V6T 2A3*
(Received 25 April 2004; published 26 August 2004)

We carry out Faddeev calculations of three-alpha (3α) and two-alpha plus Λ ($\alpha\alpha\Lambda$) systems, using two-cluster resonating-group method kernels. The input includes an effective two-nucleon force for the $\alpha\alpha$ resonating-group method and a new effective ΛN force for the $\Lambda\alpha$ interaction. The latter force is a simple two-range Gaussian potential for each spin-singlet and triplet state, generated from the phase-shift behavior of the quark-model hyperon-nucleon interaction, fss2, by using an inversion method based on supersymmetric quantum mechanics. Owing to the exact treatment of the Pauli-forbidden states between two α clusters, the present three-cluster Faddeev formalism can describe the mutually related, $\alpha\alpha$, 3α, and $\alpha\alpha\Lambda$ systems, in terms of a unique set of the baryon-baryon interactions. For the three-range Minnesota force which describes the $\alpha\alpha$ phase shifts quite accurately, the ground-state and excitation energies of ${}^{9}_{\Lambda}$Be are reproduced within 100–200 keV accuracy.

DOI: 10.1103/PhysRevC.70.024002 PACS number(s): 21.45.+v, 21.30.−x, 13.75.Cs, 12.39.Jh

I. INTRODUCTION

In spite of much effort to incorporate microscopic features of the alpha-alpha ($\alpha\alpha$) interaction, a consistent description of the three-alpha (3α) and two-alpha plus Λ ($\alpha\alpha\Lambda$) systems has not yet been obtained in the Faddeev formalism. The most favorable description of the $\alpha\alpha$ system is the $\alpha\alpha$ resonating-group method (RGM) [1]. Although some of the previous works deal with the $\alpha\alpha$ RGM kernel explicitly in the 3α-cluster Faddeev formalism, they usually yield a large overbinding for the ground state and sometimes involve spurious states because of an incomplete treatment of the Pauli-forbidden states in the 3α model space [2–5]. Various types of 3α orthogonality condition models (OCM) [6–8] also yield a similar overbinding for the ground state, although the effect of the Pauli principle between α clusters is satisfactorily treated in each framework. Only one exception to this rule is the 3α OCM in Refs. [9,10], in which the Pauli forbidden components described by the $\alpha\alpha$ bound-state solutions of the deep Buck, Friedrich, and Wheatley (BFW) potential [11] are completely eliminated. The result is rather similar to the traditional 3α Faddeev calculation using Ali-Bodmer phenomenological $\alpha\alpha$ potential with a repulsive core [12]. In these calculations, the ground-state energy of the 3α system is less than 1.5 MeV, and a simultaneous description of the compact shell-model-like ground state and the excited 0^+ state with well-developed cluster structure is not possible. The origin of the different conclusions in Refs. [8–10] is spelled out in Ref. [13], in which the existence of almost forbidden Faddeev components inherent to this 3α OCM using the bound-state Pauli-forbidden states of the BFW potential is essential.

A possible resolution of this overbinding problem of the 3α model is found in our new three-cluster Faddeev formalism, which uses singularity-free T-matrices (RGM T-matrices) generated from the two-cluster RGM kernels [14]. In this formalism, solving the Faddeev equation automatically guarantees the elimination of the three-cluster redundant components from the total wave function. The explicit energy dependence inherent in the exchange RGM kernel is self-consistently treated. We first applied this formalism to the three-dineutron and 3α systems, and obtained complete agreement between the Faddeev calculations and variational calculations using the translationally invariant harmonic-oscillator (h.o.) basis [14,15]. Next, this formalism was applied to a Faddeev calculation of the three-nucleon bound state [16], which employs complete off-shell T-matrices derived from the non-local and energy-dependent RGM kernels of the quark-model NN interactions, FSS [17] and fss2 [18]. The fss2 model yields a triton binding energy $B_t = 8.519$ MeV in the 50 channel calculation, when the np interaction is employed for all the NN pairs in the isospin basis [19]. The effect of the charge dependence of the two-body NN interaction is estimated to be -0.19 MeV for the triton binding energy [20]. This implies that our result is not overbinding in comparison with the empirical value, $B_t^{\rm exp} = 8.482$ MeV. If we attribute the difference, 0.15 MeV, to the effect of the three-nucleon force, it is by far smaller than the generally accepted values, 0.5–1 MeV [21], predicted by many Faddeev calculations employing modern realistic meson-theoretical NN interactions. We have further applied this three-cluster Faddeev formalism to the hypertriton system [22], in which the quark-model hyperon-nucleon (YN) interactions of fss2 yield a reasonable result of the hypertriton properties similar to the Nijmegen soft-core potential NSC89 [23]. Most mathematical details for the Faddeev

*Electronic address: fujiwara@ruby.scphys.kyoto-u.ac.jp

equations, employed in this calculation, are given in the present paper.

Here we apply the present three-cluster Faddeev formalism to the $\alpha\alpha\Lambda$ model for ${}^{9}_{\Lambda}$Be. This hypernucleus plays an important role to study the ΛN interaction in the *p*-shell Λ-hypernuclei. From the early time of the hypernuclear study, ${}^{9}_{\Lambda}$Be is considered to be a prototype of α-cluster structure, in which the two α clusters form a loosely bound subsystem by the effect of the extra Λ hyperon [24]. Since the *YN* interaction is usually weaker than the *NN* interaction, this system is suitable for studying a subtle structure change of the two-α system from ^{8}Be. In fact, in addition to the $1/2^{+}$ ground state [25–28] with the Λ-separation energy $B_{\Lambda}({}^{9}_{\Lambda}\mathrm{Be}) = 6.71 \pm 0.04$ MeV [29], the recent γ-ray spectroscopy [30,31] has revealed the existence of two narrow resonances in the excited states, which are supposed to be $5/2^{+}$ and $3/2^{+}$ states generated from the small spin-orbit splitting in the weak coupling picture of ${}^{8}\mathrm{Be}(2^{+}) \times \Lambda$ (spin $S = 1/2$). From a theoretical point of view, this is the simplest nontrivial system which requires the Faddeev formalism with two identical particles, involving three Pauli-forbidden states between two clusters. Several model calculations were already done with various frameworks and two-body potentials. Hiyama *et al.* [7] used the OCM for the $\alpha\alpha$, 3α and $\alpha\alpha\Lambda$ systems and discussed not only the ground state of ${}^{9}_{\Lambda}$Be, but also the spin-orbit splitting of the $5/2^{+}$ and $3/2^{+}$ states [32]. They employed simple three-range Gaussian potentials for the ΛN interaction based on *G*-matrix calculations [33] of various Nijmegen and Jülich *YN* one-boson-exchange-potential (OBEP) models. The $\Lambda\alpha$ potentials are generated from these ΛN effective potentials by the folding procedure with respect to the $(0s)^4$ h.o. wave function of the α cluster. They introduced a three-α force and adjusted the *YN* parameters to reproduce the binding energies of the ^{12}C and ${}^{9}_{\Lambda}$Be ground states. Filikhin and Gal [34] used the Faddeev and Faddeev-Yakubovsky formalisms to calculate the ${}^{9}_{\Lambda}$Be and ${}^{10}_{\Lambda\Lambda}$Be ground states. They used the Ali-Bodmer $\alpha\alpha$ potential [12] and the so-called Isle potential [35] for the $\Lambda\alpha$ interaction. They included only *S* wave in the calculation, and reproduced the ${}^{9}_{\Lambda}$Be ground-state energy correctly. However, if one includes higher partial waves the Ali-Bodmer $\alpha\alpha$ potential yields overbinding for ${}^{9}_{\Lambda}$Be by more than 0.5 MeV. Oryu *et al.* [36] carried out an $\alpha\alpha\Lambda$ Faddeev calculation by using the $\alpha\alpha$ RGM kernel and various types of $\Lambda\alpha$ potentials in the separable expansion method. Their energy spectrum of ${}^{9}_{\Lambda}$Be is reasonable, but the treatment of the two-α Pauli principle in the $\alpha\alpha\Lambda$ system is only approximate. Since they neglected the Coulomb force, a detailed comparison between their calculated results and experiment is not possible. Cravo, Fonseca, and Koike [37] performed $\alpha\alpha\Lambda$ and $\alpha\alpha n$ Faddeev calculations by using many $\alpha\alpha$ and $\Lambda\alpha$ potentials with the Coulomb force included between the two α particles. From the comparison of the results for the ${}^{9}_{\Lambda}$Be and ^{9}Be systems, they found an interesting sign change of the quadrupole moments and the magnetic moments for some excited states. They also pointed out a possibility of negative parity resonances with ${}^{5}_{\Lambda}\mathrm{He} + \alpha$ cluster structure in this threshold region.

Our purpose for the $\alpha\alpha\Lambda$ Faddeev calculations using $\alpha\alpha$ RGM kernels is threefold. First, we develop a general three-cluster Faddeev formalism with two identical clusters, in order to apply it to more complex three-cluster systems like the hypertriton interacting via quark-model baryon-baryon interactions. In the hypertriton system, we have to deal with the ΛNN-ΣNN coupled-channel system which involves a Pauli-forbidden state at the quark level in the ΛN-ΣN subsystem. Since the baryon-baryon interactions in the quark model are formulated in the two-cluster RGM formalism, the present three-cluster formalism is most appropriate to correlate the baryon-baryon interactions with the structure of few-baryon systems. The second purpose is to make a consistent description of the $\alpha\alpha$, 3α and $\alpha\alpha\Lambda$ systems using effective *NN* and ΛN interactions. This attempt is beyond the scope of the usual OCM framework and the Faddeev formalism assuming only inter-cluster potentials. A comparison of the present 3α results with the fully microscopic 3α RGM or GCM [38–40] is useful to examine the approximations involved in the present three-cluster formalism. The third purpose is to present a tractable effective ΛN force for cluster calculations of various *p*-shell hypernuclei, which is not purely phenomenological but derived microscopically from quark-model baryon-baryon interactions. In particular, this effective ΛN force should be able to reproduce the correct Λ-separation energy of ${}^{5}_{\Lambda}$He; $B_{\Lambda}({}^{5}_{\Lambda}\mathrm{He}) = 3.12 \pm 0.02$ MeV. Such a $\Lambda\alpha$ interaction is indispensable for, e.g., a $\Lambda\Lambda\alpha$ Faddeev calculation using the quark-model $\Lambda\Lambda$ interaction [41]. In this paper, we derive an effective ΛN force of two-range Gaussian form from the phase-shift behavior of the quark-model *YN* interaction, fss2, by using an inversion method based on supersymmetric quantum mechanics [42].

This paper is organized as follows. In the next section, the three-cluster Faddeev formalism with two identical clusters is given, together with expressions to calculate the expectation values of the two-cluster Hamiltonian with respect to the solutions resulting from the Faddeev equations. The procedure to calculate the $\Lambda\alpha$ and $\alpha\alpha$ *T*-matrices is also discussed, as well as the treatment of the cut-off Coulomb force employed in this paper. In the third section, we first briefly discuss the results of the 3α Faddeev calculation, and then those of the $\alpha\alpha\Lambda$ Faddeev calculation. The final section is devoted to a summary. Appendix A gives a brief comment on the rearrangement factors of three-body systems with two identical particles. The most general case with explicit spin-isospin degrees of freedom is discussed. In Appendix B, we derive a compact formula to calculate the $\Lambda\alpha$ Born kernel for arbitrary types of ΛN interactions. Energies are in MeV and lengths in fm throughout, unless otherwise specified.

II. FORMULATION

A. Faddeev equation for systems with two identical clusters

In order to formulate the Faddeev equation for systems with two identical particles, we follow the notation of Refs. [43,44] as much as possible. The Jacobi-coordinate vectors are specified by the permutation $(\alpha\beta\gamma)$, which is a *cyclic* permutation of (123). For example, the momentum vectors for the coordinate system γ in the unit of $\hbar$ are defined by

$$\boldsymbol{p}_{\gamma} = \frac{m_{\beta}\boldsymbol{k}_{\alpha} - m_{\alpha}\boldsymbol{k}_{\beta}}{m_{\alpha} + m_{\beta}},$$

$$\boldsymbol{q}_\gamma = \frac{1}{M}[(m_\alpha + m_\beta)\boldsymbol{k}_\gamma - m_\gamma(\boldsymbol{k}_\alpha + \boldsymbol{k}_\beta)],$$

$$\boldsymbol{P} = \boldsymbol{k}_\alpha + \boldsymbol{k}_\beta + \boldsymbol{k}_\gamma, \tag{1}$$

where $\boldsymbol{k}_\alpha$, $\boldsymbol{k}_\beta$, $\boldsymbol{k}_\gamma$ are single particle momenta of particles α, β, γ with the masses m_α, m_β, m_γ, respectively, and $M=m_\alpha+m_\beta+m_\gamma$ is the total mass. Three different sets of the Jacobi coordinates, $(\boldsymbol{p}_1,\boldsymbol{q}_1)$, $(\boldsymbol{p}_2,\boldsymbol{q}_2)$, and $(\boldsymbol{p}_3,\boldsymbol{q}_3)$, are related to each other in the standard relationship for the rearrangement. We choose the coordinate system $\gamma=3$ as the standard set of Jacobi coordinates and assume that particles 1 and 2 are the two identical particles with a common mass $m_1=m_2$. We incorporate the symmetry property for the exchange of particles 1 and 2 into the Faddeev formalism by assuming the total wave function $\Psi(\boldsymbol{p},\boldsymbol{q})$ as

$$\Psi(\boldsymbol{p}_3,\boldsymbol{q}_3) = \psi(\boldsymbol{p}_3,\boldsymbol{q}_3) \pm \varphi(-\boldsymbol{p}_1,\boldsymbol{q}_1) + \varphi(\boldsymbol{p}_2,\boldsymbol{q}_2)$$

$$\text{with}\quad \psi(-\boldsymbol{p}_3,\boldsymbol{q}_3) = \pm\,\psi(\boldsymbol{p}_3,\boldsymbol{q}_3), \tag{2}$$

where the upper (lower) sign is applied for identical bosons (fermions). The requirement $\Psi(-\boldsymbol{p},\boldsymbol{q})=\pm\Psi(\boldsymbol{p},\boldsymbol{q})$ is satisfied from this ansaz.

In the application to the $\alpha\alpha\Lambda$ system, two α clusters are numbered 1 and 2, and the Λ hyperon is numbered 3. Since the technique to handle the rearrangement of the Jacobi coordinates in the Faddeev formalism is well known [43], we only give the specification scheme of channels and the final Faddeev equation after partial-wave decomposition. We give expressions both in the *LS*-coupling and *jj*-coupling schemes for later convenience. For the ${}^{9}_{\Lambda}$Be system, the γ channel is specified by $\gamma=3$ with $(\gamma\alpha\beta)=(312)$ in Eq. (1). A set of quantum numbers in the γ-channel is specified by $\gamma=[(\lambda\ell)L1/2]JJ_z$ in the *LS*-coupling scheme and $[\lambda(\ell 1/2)j]JJ_z$ in the *jj*-coupling scheme with the angular-spin wave functions

$$\langle\hat{\boldsymbol{p}}_3,\hat{\boldsymbol{q}}_3|\gamma\rangle = \phi_{\alpha_1}\phi_{\alpha_2}\begin{cases}[Y_{(\lambda\ell)L}(\hat{\boldsymbol{p}}_3,\hat{\boldsymbol{q}}_3)\xi_{1/2}(3)]_{JJ_z} & (LS\text{-coupling})\\ [Y_\lambda(\hat{\boldsymbol{p}}_3)[Y_\ell(\hat{\boldsymbol{q}}_3)\xi_{1/2}(3)]_j]_{JJ_z} & (jj\text{-coupling}).\end{cases} \tag{3}$$

Here, $Y_{(\lambda\ell)LL_z}(\hat{\boldsymbol{p}},\hat{\boldsymbol{q}})=[Y_\lambda(\hat{\boldsymbol{p}})Y_\ell(\hat{\boldsymbol{q}})]_{LL_z}$, $\xi_{1/2}(3)$ is the spin wave function of Λ, and ϕ_α is the internal wave function of the α cluster. Similarly, we define the β channel by $\beta=2$ with $(\beta\gamma\alpha)=(231)$, and a set of quantum numbers $\beta=[(\ell_1\ell_2)L1/2]JJ_z$ (*LS*-coupling) and $[(\ell_1 1/2)I\ell_2]JJ_z$ (*jj*-coupling) with

$$\langle\hat{\boldsymbol{p}}_2,\hat{\boldsymbol{q}}_2|\beta\rangle = \phi_{\alpha_1}\phi_{\alpha_2}\begin{cases}[Y_{(\ell_1\ell_2)L}(\hat{\boldsymbol{p}}_2,\hat{\boldsymbol{q}}_2)\xi_{1/2}(3)]_{JJ_z} & (LS\text{-coupling})\\ [[Y_{\ell_1}(\hat{\boldsymbol{p}}_2)\xi_{1/2}(3)]_I Y_{\ell_2}(\hat{\boldsymbol{q}}_2)]_{JJ_z} & (jj\text{-coupling}).\end{cases} \tag{4}$$

The α channel is specified by $\alpha=1$ with $(\alpha\beta\gamma)=(123)$, and the quantum numbers similar to those of the β channel. The partial-wave decomposed Faddeev equation for the two components ψ and φ in Eq. (2) is given by

$$\psi_\gamma(p,q) = \left[E - \frac{\hbar^2}{4M_N}\left(p^2 + \frac{8+\zeta}{4\zeta}q^2\right)\right]^{-1}\int_0^\infty q'^2dq' \times\int_{-1}^{1}dx\langle p|\widetilde{T}_\lambda\left(E - \frac{\hbar^2}{4M_N}\frac{8+\zeta}{4\zeta}q^2,\varepsilon_\gamma\right)|p_1\rangle \times\sum_\beta \frac{1}{p_1{}^{\lambda}}g_{\gamma\beta}(q,q';x)\frac{1}{p_2{}^{\ell_1}}\varphi_\beta(p_2,q'), \tag{5a}$$

$$\varphi_\beta(p,q) = \left[E - \frac{\hbar^2}{8M_N}\left(\frac{4+\zeta}{\zeta}p^2 + \frac{8+\zeta}{4+\zeta}q^2\right)\right]^{-1}\frac{1}{2}\int_0^\infty q'^2dq' \times\int_{-1}^{1}dx\Bigg\{\langle p|T_{\ell_1}\left(E - \frac{\hbar^2}{8M_N}\frac{8+\zeta}{4+\zeta}q^2\right)|p_1'\rangle \times\sum_\gamma \frac{1}{p_1'{}^{\ell_1}}g_{\beta\gamma}(q,q';x)\frac{1}{p_2'{}^{\lambda}}\psi_\gamma(p_2',q') + \langle p|T_{\ell_1}\left(E - \frac{\hbar^2}{8M_N}\frac{8+\zeta}{4+\zeta}q^2\right)|\tilde{p}_1\rangle \times\sum_{\beta'}\frac{1}{\tilde{p}_1{}^{\ell_1}}g_{\beta\beta'}(q,q';x)\frac{1}{\tilde{p}_2{}^{\ell_1'}}\varphi_{\beta'}(\tilde{p}_2,q')\Bigg\}, \tag{5b}$$

where $\zeta=(M_\Lambda/M_N)$ is the mass ratio of Λ to the nucleon and

$$p_1 = p\left(q',\frac{1}{2}q;x\right),\quad p_2 = p\left(q,\frac{\zeta}{4+\zeta}q';x\right),$$

$$p_1' = p\left(q',\frac{\zeta}{4+\zeta}q;x\right),\quad p_2' = p\left(q,\frac{1}{2}q';x\right),$$

$$\tilde{p}_1 = p\left(q',\frac{4}{4+\zeta}q;x\right),\quad \tilde{p}_2 = p\left(q,\frac{4}{4+\zeta}q';x\right), \tag{5c}$$

with $p(q,q';x)\equiv\sqrt{q^2+q'^2+2qq'x}$. The T-matrices, $\widetilde{T}_\lambda$ and T_{ℓ_1}, are discussed in Secs. II D and II C. The rearrangement factors for the $\psi-\varphi$ or $\varphi-\psi$ cross terms are given by

$$g_{\gamma\beta}(q,q';x) = g_{\beta\gamma}(q',q;x) = \sum_{\lambda_1+\lambda_2=\lambda}\ \sum_{\lambda_1'+\lambda_2'=\ell_1} q^{\lambda_1'+\lambda_2}q'^{\lambda_1+\lambda_2'}\left(\frac{1}{2}\right)^{\lambda_2}\left(\frac{\zeta}{4+\zeta}\right)^{\lambda_2'} \times\sum_k (2k+1)g_{\gamma\beta}^{\lambda_1\lambda_1'k}P_k(x), \tag{6}$$

where $P_k(x)$ is the Legendre polynomial of rank k. The reduced rearrangement factor $g_{\gamma\beta}^{\lambda_1\lambda_1'k}$ is expressed as

$$g_{\gamma\beta}^{\lambda_1\lambda_1'k}=\begin{cases}(-1)^{\lambda}G_{(\lambda\ell),(\ell_1\ell_2)}^{\lambda_1\lambda_1'kL} & (LS\text{-coupling})\\ \sum_L(-1)^{I+J+L+\ell_1+1}\hat{j}\hat{I}(\hat{L})^2\begin{Bmatrix} j & \ell & \frac{1}{2}\\ L & J & \lambda\end{Bmatrix}\begin{Bmatrix} J & L & \frac{1}{2}\\ \ell_1 & I & \ell_2\end{Bmatrix}G_{(\lambda\ell),(\ell_1\ell_2)}^{\lambda_1\lambda_1'kL} & (jj\text{-coupling})\end{cases}, \tag{7}$$

with $\hat{j}=\sqrt{2j+1}$, etc., and the spatial angular-momentum factor $G_{(\lambda\ell),(\ell_1\ell_2)}^{\lambda_1\lambda_1'kL}$ in Eq. (A9). For the $\varphi-\varphi$ type rearrangement, these factors are given by

$$g_{\beta\beta'}(q,q';x)=\sum_{\lambda_1+\lambda_2=\ell_1}\sum_{\lambda_1'+\lambda_2'=\ell_1'}q^{\lambda_1'+\lambda_2}q'^{\lambda_1+\lambda_2'}\left(\frac{4}{4+\zeta}\right)^{\lambda_2+\lambda_2'}\sum_k(2k+1)g_{\beta\beta'}^{\lambda_1\lambda_1'k}P_k(x), \tag{8}$$

with

$$g_{\beta\beta'}^{\lambda_1\lambda_1'k}=\begin{cases}(-1)^{\ell_1+\ell_1'}G_{(\ell_1\ell_2),(\ell_1'\ell_2')}^{\lambda_1\lambda_1'kL} & (LS\text{-coupling})\\ \sum_L(-1)^{I-I'}\hat{I}\hat{I}'(\hat{L})^2\begin{Bmatrix} J & L & \frac{1}{2}\\ \ell_1 & I & \ell_2\end{Bmatrix}\begin{Bmatrix} J & L & \frac{1}{2}\\ \ell_1' & I' & \ell_2'\end{Bmatrix}G_{(\ell_1\ell_2),(\ell_1'\ell_2')}^{\lambda_1\lambda_1'kL} & (jj\text{-coupling})\end{cases}. \tag{9}$$

B. Calculation of ε_γ and ε_β

In this section, we derive some formulas to calculate expectation values of the two-cluster Hamiltonians, $h_\gamma+V_\gamma^{\mathrm{RGM}}(\varepsilon_\gamma)$ and $h_\beta+V_\beta$, where h_γ is the kinetic-energy operator of the γ pair, etc. In the present application, $V_\gamma^{\mathrm{RGM}}(\varepsilon_\gamma)$ is the $\alpha\alpha$ RGM kernel and V_β is the $\Lambda\alpha$ kernel. We deal with the energy dependence of the $\alpha\alpha$ RGM kernel self-consistently by calculating

$$\varepsilon_\gamma=\langle\Psi|h_\gamma+V_\gamma^{\mathrm{RGM}}(\varepsilon_\gamma)|\Psi\rangle \tag{10}$$

for the normalized Faddeev solution Ψ. The potential term of the matrix element in Eq. (10) is most easily obtained from various matrix elements of the kinetic-energy operators. Suppose Ψ is a sum of three Faddeev components, $\Psi=\psi_\alpha+\psi_\beta+\psi_\gamma$. Then the Faddeev equation $(E-H_0)\psi_\gamma=V_\gamma\Psi$ with $V_\gamma=V_\gamma^{\mathrm{RGM}}(\varepsilon_\gamma)$ and $H_0=h_\gamma+h_{\overline{\gamma}}$ yields $\langle\Psi|V_\gamma|\Psi\rangle=\langle\psi_\gamma|E-H_0|\Psi\rangle$. Thus Eq. (10) becomes

$$\varepsilon_\gamma=E\langle\psi_\gamma|\Psi\rangle-\langle\psi_\gamma|H_0|\Psi\rangle+\langle\Psi|h_\gamma|\Psi\rangle. \tag{11}$$

We can write a similar equation also for the β pair. We calculate ε_β, although the self-consistent procedure is not necessary for the $\Lambda\alpha$ interaction. The kinetic energy term $\langle\Psi|h_\beta|\Psi\rangle$ is obtained from $\langle\Psi|h_\gamma|\Psi\rangle$ as follows. Using the momentum Jacobi coordinates in Eq. (1), we can easily show

$$(m_\beta+m_\gamma)h_\alpha+(m_\gamma+m_\alpha)h_\beta+(m_\alpha+m_\beta)h_\gamma=MH_0. \tag{12}$$

For two identical particles with $m_\alpha=m_\beta$, this relationship yields

$$h_\alpha+h_\beta=\frac{M}{m_\beta+m_\gamma}H_0-\frac{2m_\beta}{m_\beta+m_\gamma}h_\gamma, \tag{13}$$

and

$$\langle\Psi|h_\beta|\Psi\rangle=\frac{M}{2(m_\beta+m_\gamma)}\langle\Psi|H_0|\Psi\rangle-\frac{m_\beta}{m_\beta+m_\gamma}\langle\Psi|h_\gamma|\Psi\rangle. \tag{14}$$

Thus we find, for the $\alpha\alpha\Lambda$ system,

$$\varepsilon_\beta=E\langle\psi_\beta|\Psi\rangle+\frac{8+\zeta}{2(4+\zeta)}\langle\psi_\gamma|H_0|\Psi\rangle+\frac{4}{4+\zeta}[\langle\psi_\beta|H_0|\Psi\rangle-\langle\Psi|h_\gamma|\Psi\rangle]. \tag{15}$$

We need to calculate the overlap matrix elements $\langle\psi_\gamma|\Psi\rangle$, $\langle\psi_\beta|\Psi\rangle$, and $\langle\psi_\gamma|H_0|\Psi\rangle=\langle\psi_\gamma|H_0|\psi_\gamma\rangle+2\langle\psi_\gamma|H_0|\psi_\beta\rangle$, $\langle\psi_\beta|H_0|\Psi\rangle=\langle\psi_\gamma|H_0|\psi_\beta\rangle+\langle\psi_\beta|H_0|\psi_\beta+\psi_\alpha\rangle$, $\langle\Psi|h_\gamma|\Psi\rangle=\langle\psi_\gamma|h_\gamma|\psi_\gamma\rangle+4\langle\psi_\gamma|h_\gamma|\psi_\beta\rangle+2\langle\psi_\beta|h_\gamma|\psi_\beta+\psi_\alpha\rangle$. These are calculated from ψ and φ by using the recoupling techniques developed in Appendix A. The final result is

$$\langle\psi_\gamma|H_0|\Psi\rangle=\sum_\gamma\int_0^\infty p^2dpq^2dq\frac{\hbar^2}{4M_N}\left(p^2+\frac{8+\zeta}{4\zeta}q^2\right)[\psi_\gamma(p,q)]^2+\sum_{\gamma,\beta}\int_0^\infty q^2dqq'^2dq'\int_{-1}^1dx\psi_\gamma(p_1,q)\frac{\hbar^2}{4M_N}$$
$$\times\left(p_1{}^2+\frac{8+\zeta}{4\zeta}q^2\right)\frac{1}{p_1{}^\lambda}g_{\gamma\beta}(q,q';x)\frac{1}{p_2{}^{\ell_1}}\varphi_\beta(p_2,q'), \tag{16a}$$

$$\langle\psi_\beta|H_0|\Psi\rangle = \sum_\beta \int_0^\infty p^2dpq^2dq\frac{\hbar^2}{8M_N}\left(\frac{4+\zeta}{\zeta}p^2+\frac{8+\zeta}{4+\zeta}q^2\right)[\varphi_\beta(p,q)]^2+\frac{1}{2}\sum_{\beta,\beta'}\int_0^\infty q^2dqq'^2dq'\int_{-1}^1 dx\varphi_\beta(\tilde{p}_1,q)\frac{\hbar^2}{8M_N}$$
$$\times\left(\frac{4+\zeta}{\zeta}\tilde{p}_1^{\,2}+\frac{8+\zeta}{4+\zeta}q^2\right)\frac{1}{\tilde{p}_1^{\,\ell_1}}g_{\beta\beta'}(q,q';x)\frac{1}{\tilde{p}_2^{\,\ell_1'}}\varphi_{\beta'}(\tilde{p}_2,q')+\frac{1}{2}\sum_{\gamma,\beta}\int_0^\infty q^2dqq'^2dq'\int_{-1}^1 dx\psi_\gamma(p_1,q)\frac{\hbar^2}{4M_N}$$
$$\times\left(p_1^{\,2}+\frac{8+\zeta}{4\zeta}q^2\right)\frac{1}{p_1^{\,\lambda}}g_{\gamma\beta}(q,q';x)\frac{1}{p_2^{\,\ell_1}}\varphi_\beta(p_2,q'). \tag{16b}$$

The overlap integrals are obtained by setting $H_0\to 1$. Furthermore, $\langle\Psi|h_\gamma|\Psi\rangle$ is given by

$$\langle\Psi|h_\gamma|\Psi\rangle = \sum_\gamma\int_0^\infty p^2dpq^2dq\frac{\hbar^2}{4M_N}p^2[\psi_\gamma(p,q)]^2+\sum_{\gamma,\beta}\int_0^\infty q^2dqq'^2dq'\int_{-1}^1 dx\psi_\gamma(p_1,q)\frac{\hbar^2}{2M_N}p_1^{\,2}\frac{1}{p_1^{\,\lambda}}g_{\gamma\beta}(q,q';x)\frac{1}{p_2^{\,\ell_1}}\varphi_\beta(p_2,q')$$
$$+\sum_{\beta,\beta'}\int_0^\infty p^2dpq^2dq\varphi_\beta(p,q)\frac{\hbar^2}{8M_N}\left\{\left[p^2+\left(\frac{8+\zeta}{4+\zeta}\right)^2q^2\right]\delta_{\beta,\beta'}+\frac{2(8+\zeta)}{4+\zeta}pqf_{\beta\beta'}\right\}\varphi_{\beta'}(p,q)$$
$$+\sum_{\beta,\beta'}\int_0^\infty q^2dqq'^2dq'\int_{-1}^1 dx\varphi_\beta(\tilde{p}_1,q)\frac{\hbar^2}{16M_N}(q^2+q'^2-2qq'x)\frac{1}{\tilde{p}_1^{\,\ell_1}}g_{\beta\beta'}(q,q';x)\frac{1}{\tilde{p}_2^{\,\ell_1'}}\varphi_{\beta'}(\tilde{p}_2,q'). \tag{17}$$

Here, $f_{\beta\beta'}$ is given by

$$f_{\beta\beta'}=\int d\hat{\mathbf{p}}_2d\hat{\mathbf{q}}_2\langle\beta|\hat{\mathbf{p}}_2\hat{\mathbf{q}}_2\rangle(\hat{\mathbf{p}}_2\cdot\hat{\mathbf{q}}_2)\langle\hat{\mathbf{p}}_2\hat{\mathbf{q}}_2|\beta'\rangle=(-1)^{\ell_1+\ell_2'}\hat{\ell}_1\hat{\ell}_2\langle\ell_1010|\ell_1'0\rangle\langle\ell_2010|\ell_2'0\rangle$$
$$\times\begin{cases}(-1)^L\begin{Bmatrix}\ell_1 & \ell_2 & L\\ \ell_2' & \ell_1' & 1\end{Bmatrix} & (LS\text{-coupling})\\ \sum_L(-1)^{I-I'+L}\hat{I}\hat{I}'(\hat{L})^2\begin{Bmatrix}J & L & \frac{1}{2}\\ \ell_1 & I & \ell_2\end{Bmatrix}\begin{Bmatrix}J & L & \frac{1}{2}\\ \ell_1' & I' & \ell_2'\end{Bmatrix}\begin{Bmatrix}\ell_1 & \ell_2 & L\\ \ell_2' & \ell_1' & 1\end{Bmatrix} & (jj\text{-coupling}).\end{cases} \tag{18}$$

C. $\Lambda\alpha$ *T*-matrix and effective ΛN potentials

The $\Lambda\alpha$ *T*-matrices are obtained by solving the Lippmann-Schwinger equation

$$T_\ell(p,p';E)=V_\ell(p,p')-\frac{4\pi}{(2\pi)^3}\frac{2\mu}{\hbar^2}\int_0^\infty k^2dkV_\ell(p,k)$$
$$\times\frac{1}{\gamma^2+k^2}T_\ell(k,p';E), \tag{19}$$

where $\mu=[4\zeta/(4+\zeta)]M_N$ is the $\Lambda\alpha$ reduced mass and $E=-(\hbar^2/2\mu)\gamma^2$ is a negative energy. The partial-wave components $V_\ell(p,p')$ for the $\Lambda\alpha$ Born kernel $V(\mathbf{p},\mathbf{p}')$ are defined through

$$V(\mathbf{p},\mathbf{p}')=4\pi\sum_\ell V_\ell(p,p')\sum_m Y_{\ell m}(\hat{\mathbf{p}})^*Y_{\ell m}(\hat{\mathbf{p}}'), \tag{20}$$

and the $\langle p|T_\ell(E)|p'\rangle$ in Eq. (5b) is related to $T_\ell(p,p';E)$ with an extra factor $4\pi/(2\pi)^3$.

For the effective ΛN potential, we assume a Minnesota-type central force [45]

$$v_{\Lambda N}=\left[v(^1E)\frac{1-P_\sigma}{2}+v(^3E)\frac{1+P_\sigma}{2}\right]\left[\frac{u}{2}+\frac{2-u}{2}P_r\right], \tag{21}$$

where $v(^1E)$ and $v(^3E)$ are simple two-range Gaussian potentials generated from the $^1S_0$ and $^3S_1$ phase shifts predicted by the quark-model ΛN interaction, fss2. We use the inversion method based on supersymmetric quantum mechanics, developed in Ref. [42], to derive phase-shift equivalent local potentials. These potentials are then fitted by two-range Gaussian functions. These are given by

$$v(^1S_0)=-128.0\exp(-0.8908r^2)+1015\exp(-5.383r^2),$$
$$v(^3S_1)=-56.31f\exp(-0.7517r^2)+1072\exp(-13.74r^2), \tag{22}$$

where $f=1$ and r is the relative distance between Λ and N. In the following, we call this effective ΛN potential the SB potential. Figure 1 shows that these potentials fit the low-energy behavior of the $^1S_0$ and $^3S_1$ ΛN phase shifts obtained by the full ΛN-ΣN coupled-channel RGM calculations of fss2. In the $^3S_1$ state, only the low-energy region is fitted, since the cusp region cannot be fitted in a single-channel

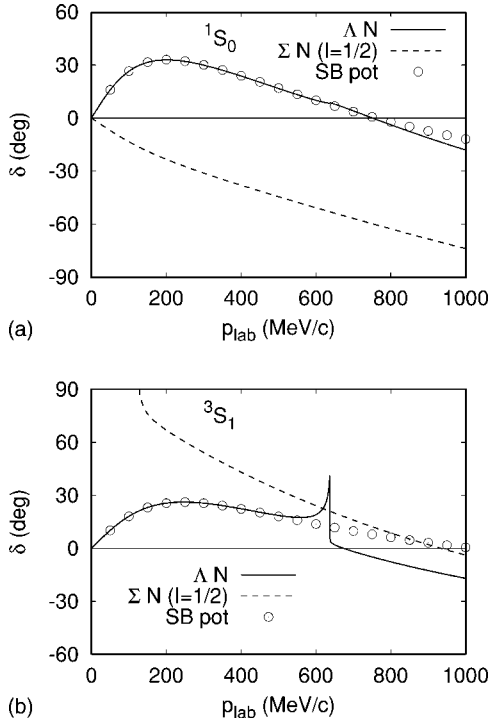

FIG. 1. ΛN-ΣN $^1S_0$ (a) and $^3S_1$ (b) phase shifts for the isospin $I=1/2$ channel, calculated with fss2 [46] (solid and dashed curves) and with the SB potential (circles).

calculation. This potential overestimates the $^3S_1$ phase shift in the higher energy region. The procedure to calculate the $\Lambda\alpha$ Born kernel for the simple $(0s)^4$ α-cluster wave function is discussed in Appendix B. Here we only give the final result for the partial-wave components:

$$V_\ell(q_f,q_i)=\sum_{i=1}^{4}[X_d^i V_\ell^d(q_f,q_i;\kappa_i)+X_e^i V_\ell^e(q_f,q_i;\kappa_i)]. \quad (23)$$

Here, X_d^i and X_e^i are spin-isospin factors defined in Eq. (B10) and tabulated in Table I for the present two-range Gaussian potentials. The explicit functional form of $V_\ell^d(q_f,q_i;\kappa_i)$ and $V_\ell^e(q_f,q_i;\kappa_i)$ are given in Eq. (B11).

In this paper, we also examine the ΛN effective forces [33] used by Hiyama *et al.* [7] for comparison. These potentials are generated from the *G*-matrix calculations of various OBEP potentials. They are parametrized as

TABLE I. $\Lambda\alpha$ spin-flavor coefficients for the Minnesota-type SB potential with $v=v_0e^{-\kappa r^2}$.

i	X_d^i	X_e^i	κ_i
1, 2	$(u/2)v_0(^1S)$	$(1-u/2)v_0(^1S)$	$\kappa(^1S)$
3, 4	$(3u/2)v_0(^3S)$	$3(1-u/2)v_0(^3S)$	$\kappa(^3S)$

TABLE II. Bound-state energies for the $\Lambda\alpha$ system, $E(^5_\Lambda\mathrm{He})$ (in MeV), calculated by the original SB potential with $f=1$. The h.o. width parameters, $\nu=0.275$ fm^{-2} and $\nu=0.257$ fm^{-2} are assumed for the $(0s)^4$ α-cluster. The experimental value is $E^{\mathrm{exp}}(^5_\Lambda\mathrm{He})=-3.12\pm0.02$ MeV.

u	$\nu=0.275$ fm^{-2}	$\nu=0.257$ fm^{-2}
1	−4.975	−4.747
0.6	−4.946	−4.728

$$v_{\Lambda N}=\sum_{i=1}^{3}\left\{[v_{0\ \mathrm{even}}^{(i)}+v_{\sigma\sigma\ \mathrm{even}}^{(i)}(\sigma_1\cdot\sigma_2)]\frac{1+P_r}{2}+[v_{0\ \mathrm{odd}}^{(i)}+v_{\sigma\sigma\ \mathrm{odd}}^{(i)}(\sigma_1\cdot\sigma_2)]\frac{1-P_r}{2}\right\}e^{-(r/\beta_i)^2}. \quad (24)$$

Since the spin-spin term does not contribute to the spin saturated α-cluster, the spin-isospin factors in Eq. (23) (with $\kappa_i\rightarrow 1/(\beta_i)^2$, $i=1-3$) are given by

$$X_d^i=2(v_{0\ \mathrm{even}}^{(i)}+v_{0\ \mathrm{odd}}^{(i)}),$$

$$X_e^i=2(v_{0\ \mathrm{even}}^{(i)}-v_{0\ \mathrm{odd}}^{(i)}). \quad (25)$$

The explicit values for $v_{0\ \mathrm{even}}^{(i)}$ and $v_{0\ \mathrm{odd}}^{(i)}$ $(i=1-3)$ generated from Nijmegen models, NS, ND, NF, and Jülich potentials, JA, JB, are given in Ref. [7]. [Table V of Ref. [7] includes a misprint for NS: the width parameters β_i for this potential are $1.50-1.0-0.55$, instead of $1.50-0.90-0.50$ for the other potentials.]

The binding energy of the $\Lambda\alpha$ bound state depends on the h.o. width parameter ν of the α-cluster. Table II shows that the SB potential of Eq. (22) overbinds the $^5_\Lambda$He energy by more than 1.6 MeV. It also shows that the u-dependence is very weak, which implies that $^5_\Lambda$He is an *S*-wave dominated system. It is well known that a central single-channel ΛN effective force that fits the low-energy ΛN total cross sections and the ground-state energies of $^3_\Lambda$H, $^4_\Lambda$H and $^4_\Lambda$He always overestimates the $^5_\Lambda$He binding energy by more than 2 MeV, due to a lack of Λ-Σ mixing and the tensor force [47–50]. In order to circumvent this difficulty, we introduce a reduction factor f in the attractive part of the $^3S_1$ potential in Eq. (22) for the following Faddeev calculations. The choices $f=0.8821$ for $\nu=0.275$ fm^{-2} and $f=0.8923$ for $\nu=0.257$ fm^{-2} reproduce the desired value $E(^5_\Lambda\mathrm{He})=-3.120$ MeV, when the pure Serber type SB potential with $u=1$ is used. The $\Lambda\alpha$ bound-state energies predicted by the NS-JB effective ΛN potentials deviate from the original fit in Ref. [7] by 110−170 keV (−3.23 to −3.29 MeV). This is because they used a slightly different expression from ours for the exchange term of the $\Lambda\alpha$ potential. For the $\alpha\alpha\Lambda$ Faddeev calculations using the Minnesota three-range force for the $\alpha\alpha$ RGM kernel ($\nu=0.257$ fm^{-2}), we readjusted the strength of the original NS-JB ΛN potentials in order to fit the precise $^5_\Lambda$He energy, −3.120 MeV. This is achieved by

slightly (less than 0.36%) modifying the strength of the short-range repulsive term (the third component) of the original G-matrix potentials.

The $\Lambda\alpha$ phase shifts are also calculated, although there is no experimental information. The S-wave phase shift shows a monotonic decrease from 180° similar to Fig. 9 of Ref. [36]. In the energy region $E_{\mathrm{c.m.}}(\Lambda\alpha)=0-20$ MeV, the phase shifts of the higher partial waves rapidly decrease, starting from 20°~30° for the P wave. This implies that the $\Lambda\alpha$ potential is very much of the Wigner type, and our lack of knowledge of the $\Lambda\alpha$ interaction in higher partial waves may not become a serious problem in the Faddeev calculations.

D. $\alpha\alpha$ T-matrix and effective NN potentials

The $\alpha\alpha$ T-matrices used for the 3α and $\alpha\alpha\Lambda$ Faddeev calculations are generated from the $\alpha\alpha$ RGM kernel which uses an effective NN potential similar to Eq. (21). In the notation used in Ref. [51], the $\alpha\alpha$ RGM kernel, $V^{\mathrm{RGM}}(\varepsilon)=V_{\mathrm{D}}+V_{\mathrm{D}}{}^{\mathrm{Cl}}+G+G^{\mathrm{Cl}}+\varepsilon K$ consists of the direct potential V_{D}, the direct Coulomb potential $V_{\mathrm{D}}{}^{\mathrm{Cl}}$, the sum of the exchange kinetic-energy and interaction kernels, $G=G^{\mathrm{K}}+G^{\mathrm{V}}$, the exchange Coulomb kernel G^{Cl}, and the exchange normalization kernel K. We have to eliminate redundant components from the energy-dependent partial wave T-matrices, $T_\lambda(p,p';E,\varepsilon)$, which satisfy the Lippmann-Schwinger equation similar to Eq. (19). This is necessary only for the S-wave ($\lambda=0$) and D-wave ($\lambda=2$) components, for which there exist two and one h.o. Pauli redundant states, $u_{n\lambda}(p)$, respectively. Here, $u_{n\lambda}(p)$ are essentially the h.o. wave functions in the momentum representation with the total h.o. quanta $N=2n+\lambda=0$ and 2, satisfying $Ku_{n\lambda}=u_{n\lambda}$. They are explicitly given by

$$u_{n\lambda}(p)=(-1)^n\frac{(2\pi)^{3/2}}{\sqrt{4\pi}}R_{n\lambda}\left(p,\frac{1}{4\mu\nu}\right) \tag{26}$$

with $\mu=2$, in terms of the standard three-dimensional h.o. radial wave function $R_{n\ell}(r,\nu)$ in the coordinate representation. The RGM T-matrices defined in Ref. [14] are calculated by

$$\widetilde{T}_\lambda(p,p';E,\varepsilon)=T_\lambda(p,p';E,\varepsilon)+\frac{\hbar^2}{4M_N}\frac{(\gamma^2+p^2)(\gamma^2+p'^2)}{(\gamma^2+\kappa^2)}\times\begin{cases}\sum_{n=0}^{1}u_{n0}(p)u_{n0}(p')\\ u_{02}(p)u_{02}(p')\end{cases}$$

$$\text{for }\lambda=\begin{cases}0\\2\end{cases}, \tag{27}$$

where $\gamma^2=-(4M_NE/\hbar^2)$ and $\kappa^2=(4M_N\varepsilon/\hbar^2)$. For the higher partial waves with $\lambda\geqslant 4$, we define $\widetilde{T}_\lambda(p,p';E,\varepsilon)=T_\lambda(p,p';E,\varepsilon)$. The RGM T-matrices in Eq. (27) satisfy the orthogonality condition

$$u_{n\lambda}(p)=\frac{4\pi}{(2\pi)^3}\frac{4M_N}{\hbar^2}\int_0^\infty p'^2dp'\widetilde{T}_\lambda(p,p';E,\varepsilon)\frac{u_{n\lambda}(p')}{\gamma^2+p'^2}, \tag{28}$$

for $n=0$, 1 ($\lambda=0$) and $n=0$ ($\lambda=2$). Owing to this relationship, we can prove the orthogonality of the total wave function Eq. (2) to the Pauli-forbidden states $u_{n\lambda}(p)$.

For the effective NN force, we mainly use the three-range Minnesota (MN) force [45] with the exchange-mixture parameter, $u=0.946\,87$, and the h.o. width parameter, $\nu=0.257$ fm^{-2}, for the $(0s)^4$ α-clusters. We also use the two-range Volkov No.1 (VN1) and No.2 (VN2) forces [52], in order to comapre our 3α results with the microscopic RGM [38,53] and GCM [39] calculations. The Majorana parameters m of the Volkov forces and the h.o. width parameters are $m=0.575$ and $\nu=0.2515$ fm^{-2} for VN1, and $m=0.59$ and $\nu=0.275$ fm^{-2} for VN2. The $\alpha\alpha$ RGM calculations using these effective NN forces and the complete Coulomb kernel reasonably reproduce the empirical $\alpha\alpha$ phase shifts of the S-, D-, and G-waves, as well as the S-wave resonance near the $\alpha\alpha$ threshold. However, the best fit to the experiment is obtained by the three-range MN force. For the VN2 force, the s-wave resonance appears as a bound state with the binding energy $B_{\alpha\alpha}=245$ keV. Although the VN1 force reproduces this resonance, the overall fit to the $\alpha\alpha$ phase shifts is less impressive compared to the MN force. In the RGM calculation, the precise determination of the resonance energy is not easy even in the two-α system, because of the presence of the Coulomb force. In the present Lippmann-Schwinger formalism in the momentum representation, the method by Vincent and Phatak [54] is used for solving the scattering problem with full Coulomb force at the nucleon level. We find that the 0^+ resonance energy is 0.18 and 0.14 MeV for VN1 force and the MN force, respectively. This should be compared with the experimental value 0.092 MeV.

For the Coulomb force in the 3α and $\alpha\alpha\Lambda$ Faddeev calculations, we use the cut-off Coulomb force at the nucleon level

$$v_{i,j}^{\mathrm{Cl}}(r)=\frac{1+\tau_z(i)}{2}\frac{1+\tau_z(j)}{2}\frac{e^2}{r}\theta(R_C-r), \tag{29}$$

with the cut-off radius R_C, although an exact treatment of the point Coulomb force exists for bound-state nuclear three-body problems with two charged particles [55]. Here $\theta(x)$ is the Heaviside step function. For the most compact 3α ground state, this approximation with $R_C=10$ fm is good enough to obtain 1–2 keV accuracy. The exchange Coulomb kernel for Eq. (29) is calculated analytically. The partial-wave decomposition of the $\alpha\alpha$ RGM kernel is carried out numerically using the Gauss-Legendre 20-point quadrature formula, when the Coulomb force is not included. When the cut-off Coulomb force with a $R_C=14$ fm is employed, it is increased to the 30-point quadrature formula to obtain an accuracy within 1 keV for the exchange Coulomb kernel. The direct Coulomb term is separately integrated with a sufficient number of numerical integration points.

III. RESULTS

To solve the Faddeev equation, we discretize the continuous momentum variable p (q) for the Jacobi coordinate vectors, using the Gauss-Legendre n_1-point (n_2-point) quadrature formula, for each of the three intervals of $0-1$ fm^{-1}, $1-3$ fm^{-1} and $3-6$ fm^{-1}. The small contribution from the intermediate integral over p beyond $p_0=6$ fm^{-1} in the $\alpha\alpha$ T-matrix calculation is also taken into account by using the Gauss-Legendre n_3-point quadrature formula through the mapping $p=p_0+\tan\{\pi(1+x)/4\}$. We need $n_1 \geqslant 10$ and $n_3=5$, so that 35 points are at least necessary to follow up the inner oscillations of the two-α bound-state wave function and the necessary T-matrices for solving the Faddeev equation. These n_3 points for $p>6$ fm^{-1} are, however, not included for solving the Faddeev equation, since it causes a numerical instability for the interpolation. The momentum region $q=6$ fm$^{-1}-\infty$ is also discretized by the n_3 point formula just as in the p discretization. We take n_1-n_2-n_3=15-10-5 for the 3α system and 10-10-5 for the $\alpha\alpha\Lambda$ system, respectively, unless otherwise specified. The modified spline interpolation technique developed in Ref. [56] is employed to generate the rearrangement matrices. For the large-scale diagonalization of non-symmetric matrices, the Arnoldi-Lanczos algorithm developed in the ARPACK subroutine package [57] is very useful.

A. 3α Faddeev calculation

In order to make sure that our Faddeev equation is solved correctly, we first carried out the standard 3α-particle Faddeev calculation by using the angular-momentum dependent Ali-Bodmer potential of d type (ABd). We find that the 3α energy, $E_{3\alpha}=-6.423$ MeV without Coulomb force, is consistent with previous calculations [9]. Here, we used $\hbar^2/M_\alpha = 10.4465$ MeV fm^2 and $e^2=1.44$ MeV fm for comparison. When the cut-off Coulomb force is included, our value -1.527 MeV is 4 keV lower than the -1.523 MeV given in Table I of Ref. [9]. This difference is due to a slightly different treatment of the Coulomb force between the two calculations. The small 3α binding energy implies that the Ali-Bodmer phenomenological $\alpha\alpha$ potential cannot describe the ground state of ^{12}C with a compact shell-model like structure.

On the other hand, the present 3α model interacting via the $\alpha\alpha$ RGM kernel gives enough binding and a large overlap with the compact shell-model-like component. Table III lists the results of such Faddeev calculations for the ground state of the 3α system with and without the Coulomb force. The $\alpha\alpha$ RGM kernels are generated from the VN1, VN2, and MN forces. When the Coulomb effect is included, the cut-off Coulomb force with $R_C=10$ fm is employed. In the last column in Table III, $c_{(04)}$ implies the overlap amplitude of the 3α bound-state function with the SU_3 (04) shell-model configuration. We find that all three effective NN forces yield binding energies comparable with the experimental value $|E_{3\alpha}^{\rm exp}|=7.275$ MeV, although the result of of the MN force is a little too large. The dominant component of these 3α ground states is the SU_3 (04) shell-model configuration.

TABLE III. Results of 3α Faddeev calculations, using the $\alpha\alpha$ RGM kernel, with and without the Coulomb effect. The parenthesized numbers indicate the results when the cut-off Coulomb force with $R_C=10$ fm are included at the nucleon level. Partial waves up to $\lambda_{\max}$ are included in $\alpha\alpha$ and (2α)-α channels. The heading $\varepsilon_{2\alpha}$ is the expectation value of the two-α Hamiltonian with respect to the 3α bound state solution, $E_{3\alpha}$ the 3α bound-state energy, and $c_{(04)}$ the overlap between the 3α bound-state wave function and the SU_3 (04) shell-model configuration. For the MN force, the result of the variational calculation using the translationally invariant h.o. basis (h.o. var.) is also given for comparison, where h.o. quanta up to $N=60$ are included.

Force	$\lambda_{\max}$	$\varepsilon_{2\alpha}$	$E_{3\alpha}$	$c_{(04)}$
	4	9.657 (10.887)	−10.751 (−5.206)	0.900 (0.879)
VN1	6	9.531 (10.779)	−10.926 (−5.365)	0.896 (0.875)
	8	9.530 (10.778)	−10.927 (−5.366)	0.896 (0.875)
	4	8.583 (9.608)	−11.202 (−5.781)	0.826 (0.795)
VN2	6	8.449 (9.505)	−11.415 (−5.967)	0.821 (0.790)
	8	8.447 (9.503)	−11.417 (−5.969)	0.821 (0.790)
	4	12.032 (13.603)	−15.616 (−9.433)	0.979 (0.973)
MN	6	11.905 (13.482)	−15.777 (−9.591)	0.978 (0.971)
	8	11.904 (13.481)	−15.779 (−9.592)	0.978 (0.971)
h.o. var.		11.903 (13.480)	−15.781 (−9.594)	0.978 (0.971)

In Table IV we compare the 3α ground-state energies $E_{3\alpha}$, predicted in the present three-cluster Faddeev formalism, with those obtained by fully microscopic calculations, $E_{3\alpha}^{\rm full}$. We find that the present three-cluster equation gives 3α energies which are only 1.5–1.8 MeV higher than those of the fully microscopic 3α RGM or GCM calculations. This implies that the three-cluster exchange effect, which is neglected in our three-cluster formalism, but is present in the fully microscopic three-cluster RGM kernel, is attractive in nature, and is not as large as the repulsive three-body force claimed necessary in the semi-microscopic 3α models [2,4]. This is mainly because the 3α model space used by these authors does not exclude the 3α Pauli-forbidden components

TABLE IV. Comparison of the 3α ground-state energies, predicted by the present model ($E_{3\alpha}$) and by fully microscopic calculations ($E_{3\alpha}^{\rm full}$). The experimental value is $E_{3\alpha}^{\rm exp}=-7.275$ MeV. The present model is the Faddeev calculation using the $\alpha\alpha$ RGM kernel, including the cut-off Coulomb force with $R_C=10$ fm. The heading $E_\alpha^{\rm int}$ implies the internal energy of the $(0s)^4$ α-cluster with the h.o. width parameter ν, $E_{\rm tot}$ the total energy from the RGM ([53] for MN and [38] for VN2) or GCM ([39] for VN1) calculations, and $E_{3\alpha}^{\rm full}=E_{\rm tot}-3E_\alpha^{\rm int}$.

Force	ν (fm^{-2})	$E_\alpha^{\rm int}$	$E_{\rm tot}$	$E_{3\alpha}^{\rm full}$	$E_{3\alpha}$
VN1	0.2515	−27.0	−87.9	−6.9	−5.37
VN2	0.275	−27.3	−89.4	−7.5	−5.97
MN	0.257	−23.9	−83.0	−11.4	−9.59

TABLE V. Kinetic- and potential-energy contributions to the three-α energy $E_{3\alpha}$, calculated from $\langle H_0\rangle = 2(3\varepsilon_{2\alpha} - E_{3\alpha})$ and $\langle V\rangle = 3(E_{3\alpha} - 2\varepsilon_{2\alpha})$. The shell-model (04) component, $c_{(04)}$, is large if $\langle H_0\rangle$ is large.

Force	$\varepsilon_{2\alpha}$	$E_{3\alpha}$	$\langle H_0\rangle$	$\langle V\rangle$	$c_{(04)}$
VN1	10.778	−5.366	75.402	−80.768	0.875
VN2	9.503	−5.969	68.958	−74.927	0.790
MN	13.481	−9.592	100.068	−109.660	0.971

accurately, unlike the one used in the present Faddeev formalism.

In Tables III and IV, we also find that the three-range MN force gives a somewhat large overbinding of 2–4 MeV, if the 3α energy $E_{3\alpha}$ is measured from the 3α threshold. The decomposition of the 3α energy to the kinetic-energy and potential-energy contributions in Table V implies that this overbinding is due to the large cancellation between these two contributions. In this respect, it is interesting to note that the α clusters with $\nu = 0.257$ fm^{-2} (which gives the correct rms radius $r_\alpha = (3/4\sqrt{\nu}) = 1.48$ fm [58] for the simple $(0s)^4$ α-cluster) give less binding in the framework of the orthogonality condition model (OCM) [8]. If the h.o. constant parameter ν is small, a proper treatment of the $\alpha\alpha$ exchange kernel seems to be essential in order to obtain a large binding energy of the 3α ground state. This is reasonable since the large overlap of two α-clusters implies the importance of nucleon exchange effects.

B. $\alpha\alpha\Lambda$ Faddeev calculation

For a detailed description of the $\alpha\alpha\Lambda$ bound states in the Faddeev calculation, it is important to make sure that the result is converged with respect to the following three conditions:

(1) convergence with respect to the momentum discretization points,

(2) convergence with respect to the extension of partial waves included,

(3) convergence with respect to the cut-off radius R_C, when the cut-off Coulomb force is included.

Among them, the Coulomb effect is the most difficult, since the T-matrix of the full Coulomb force is divergent at the diagonal part and the strong oscillation in the momentum representation in the cut-off Coulomb case does not lead to the correct answer, unless the numerical angular-momentum projection of the $\alpha\alpha$ Coulomb kernel (especially the direct Coulomb term) is accurately performed. As to the partial waves, we can easily enumerate all possible angular-momentum states of ${}^{9}_{\Lambda}$Be for the $L^\pi = 0^+$ ground state with $J = 1/2$ and the $L^\pi = 2^+$ excited state with $J = 5/2$ and $3/2$ in the LS coupling scheme. If no $\Lambda\alpha$ spin-orbit force is introduced, the $J = 5/2$ and $3/2$ excited states are degenerate and the LS-coupling scheme is more efficient than the jj-coupling scheme to reduce the number of channels coupled in the calculation. In the following, the angular-momentum truncation is specified by $\lambda_{\max}$-$\ell_{1_{\max}}$ values for the $\alpha\alpha$ and $\Lambda\alpha$ pairs. For example, D-P in the ground-state calculation implies a 4-channel calculation and G-G in the $L^\pi = 2^+$ calculation a 19-channel calculation. The largest model space adopted is I-I, which is an 11-channel calculation for $L^\pi = 0^+$ and a 28-channel calculation for $L^\pi = 2^+$. Note that the variational calculation in Ref. [7] uses a rather restricted model space, i.e., a 3-channel calculation with $\lambda_{\max} = 2$ and $\ell_{1_{\max}} = 0$, although the meaning of angular-momentum truncation is a little different from ours. For the momentum discretization points, we find that the energy change due to the increase of n_1-n_2-n_3 is very much R_C dependent. It is usually positive if we go from n_1-n_2-n_3 = 5-5-5 to n_1-n_2-n_3 = 10-10-5 when the Coulomb force is not included, but it turns out negative when $R_C = 10$ and 14 fm. This implies that the Faddeev calculation without Coulomb force usually overestimates the binding energy, if the number of momentum discretization points is not large enough. Since the cut-off Coulomb kernels are oscillating, too small a number of momentum discretization points such as in n_1-n_2-n_3 = 5-5-5 case is dangerous when R_C is very large like $R_C = 10$ and 14 fm. The orthogonality to the Pauli-forbidden states also deteriorates when the number of momentum discretization points is too small. The squared norm of the Pauli-forbidden components contaminating the total wave function is typically 10^{-5}–10^{-6} when n_1-n_2-n_3 = 5-5-5, but is improved to less than 10^{-13} for n_1-n_2-n_3 = 10-10-5. In this paper, we will mainly show the results of n_1-n_2-n_3 = 10-10-5, since the energy gain by further extension to n_1-n_2-n_3 = 15-15-5 is usually less than 1 keV, when the cut-off Coulomb force with $R_C = 10$–14 fm is included.

The energy gain of the ground state, ΔE, and that of the self-consistent $\varepsilon_{2\alpha}$ value by the increase of the maximum angular-momentum values, $\lambda_{\max}$-$\ell_{1_{\max}}$, are shown in Table VI in the cases when we use the VN2 or MN forces for the $\alpha\alpha$ interaction and the SB force for the $\Lambda\alpha$ interaction. In these calculations the cut-off Coulomb force with $R_C = 6$ fm is employed. If the S-wave calculation is extended to include the D-wave, the energy gain is about 1 MeV for VN2+SB and 1.2 MeV for MN+SB. The energy gain mainly comes from the partial-wave component with $\ell_1 = \ell_2 = 1$ of the α-${}^{5}_{\Lambda}$He channel. The effect of the partial wave $\ell_1 = \ell_2 = 2$ is rather small; i.e., about 50 (VN2)–60 (MN) keV. Needless to say, the exact energy gain largely depends on the character of the ΛN odd force. The ground-state energy is further improved by 7 (VN2)–5 (MN) keV and 0.03 (VN2)–0.0 (MN) keV, according to the extension to the G- and I-wave, respectively. On the other hand, $\varepsilon_{2\alpha}$ is improved by 165 (VN2)–288 (MN) keV, 6 keV and 0.5–0.6 keV, according to the extension to the D-, G- and I-waves, respectively. In conclusion, partial waves up to the D-wave are sufficient within 10 keV accuracy. If we wish to have a 1 keV accuracy, we need to take into account at least up to the G-wave. This implies that the partial-wave truncation in the Faddeev formalism is very efficient and the result converges very rapidly, according to the increase of the partial waves taken into account.

Table VII shows the R_C dependence of the two-α energy $E({}^{8}$Be), the self-consistently determined $\varepsilon_{2\alpha}$, the three-cluster ground-state energy $E({}^{9}_{\Lambda}$Be), the Λ separation energy defined by $B_\Lambda({}^{9}_{\Lambda}\text{Be}) = E({}^{8}\text{Be}) + M_\Lambda - E({}^{9}_{\Lambda}\text{Be})$, and the expecta-

TABLE VI. Energy gain for the ground state (ΔE) and that of the self-consistent $\varepsilon_{2\alpha}$ value ($\Delta\varepsilon_{2\alpha}$) in keV, for the extension of the maximum angular-momentum values, $\lambda_{\max}$-$\ell_{1\max}$. The cut-off Coulomb force with $R_C=6$ fm is included.

Force	VN2+SB				MN+SB			
	ΔE(keV)		$\Delta\varepsilon_{2\alpha}$ (keV)		ΔE (keV)		$\Delta\varepsilon_{2\alpha}$ (keV)	
n_1-n_2-n_3	5-5-5	10-10-5	5-5-5	10-10-5	5-5-5	10-10-5	5-5-5	10-10-5
S-$S\rightarrow D$-P	−954	−954	165	160	−1165	−1172	287	281
D-$P\rightarrow D$-D	−50	−50	5	5	−57	−58	7	7
D-$D\rightarrow G$-G	−7	−7	6	6	−6	−5	7	6
G-$G\rightarrow I$-I	−0.03	−0.03	0.6	0.6	−0.1	−0.0	0.5	0.5

tion value of the $\Lambda\alpha$ Hamiltonian, $\varepsilon_{\Lambda\alpha}$, when the momentum discretization points with n_1-n_2-n_3=10-10-5 and the partial waves up to I-I are used in the MN plus SB model. The energy increase (and the accumulated one) due to the increase of R_C is also shown with the plus sign in the second (and the third) row. We find that the ground-state energy $E(^9_\Lambda\mathrm{Be})$ increases by 1.621 MeV when we move from $R_C=0$ to $R_C=6$ fm, which is larger than 1.127 MeV calculated for the free two-α bound state. This seems to be natural, since the two-α subsystem is more compact in the $^9_\Lambda$Be system. The energy increase in the self-consistently determined $\varepsilon_{2\alpha}$ values is 1.435 MeV, which is about 200 keV smaller than the energy increase in $E(^9_\Lambda\mathrm{Be})$, but is still larger than in the free two-α bound state by about 300 keV. This observation is a good example that our self-consistent procedure of determining $\varepsilon_{2\alpha}$ is reasonably functioning. It is interesting to note that this large Coulomb effect in the three-body ground state; i.e., about 1.4 times larger than in the two-α system, is characteristic for the increase of R_C from 0 to 6 fm. For the range from $R_C=6$ to 10 fm, just the opposite is true and the energy increase in the three-body ground state (85 keV) is smaller than in the two-α system (>133 keV). This is apparently because the free $\alpha\alpha$ relative wave function is more widely spread than the correlated $\alpha\alpha$ relative wave function in the $^9_\Lambda$Be ground state. The tendency of $\varepsilon_{2\alpha}$ falls just into the middle of these two extremes. By using this feature, we can easily estimate the full Coulomb effect in the $E(^9_\Lambda\mathrm{Be})$ ground state. We find that the result with $R_C=10$ fm is accurate within a 1 keV error both for $E(^9_\Lambda\mathrm{Be})$ and $\varepsilon_{2\alpha}$. From Table VII, the final result for the MN+SB potentials is

$$E\left(^9_\Lambda\mathrm{Be}\right)=27.35-34.18=-6.837\ \mathrm{MeV},$$

$$\varepsilon_{2\alpha}=19.46-18.27=1.181\ \mathrm{MeV},$$

$$\varepsilon_{\Lambda\alpha}=9.215-7.954=1.261\ \mathrm{MeV},$$

$$c_{(40)}=0.695. \tag{30}$$

Here we have shown the kinetic-energy and potential-energy contributions separately in each energy, and $c_{(40)}$ is the overlap amplitude of the $^9_\Lambda$Be ground-state wave function with the shell-model (40) wave function. [Note that the sum of the $\varepsilon_{2\alpha}$ potential energy and twice of the $\varepsilon_{\Lambda\alpha}$ potential energy is the potential energy of $E(^9_\Lambda\mathrm{Be})$, but this is not true for the kinetic-energy terms.] We have also carried out the similar analysis in the VN2+SB model. The converged result of the VN2+SB forces, including the cut-off Coulomb force with $R_C=14$ fm, is given by

TABLE VII. Cut-off radius (R_C) dependence of the Coulomb energies in the two-α bound state energy $E(^8\mathrm{Be})$, the two-α expectation value $\varepsilon_{2\alpha}$, the three-body bound state energy $E(^9_\Lambda\mathrm{Be})$, the Λ separation energy $B_\Lambda(^9_\Lambda\mathrm{Be})$, and the $\Lambda\alpha$ expectation value $\varepsilon_{\Lambda\alpha}$. Calculations are carried out by using n_1-n_2-n_3=10-10-5 and the partial waves up to I-I. The three-range MN force and the SB force are used with $\nu=0.257\ \mathrm{fm}^{-2}$ for the h.o. width parameter of the α-clusters. The energy increase (and the accumulated one) due to the increase of R_C is also shown with the plus sign in the second (and third) row. The experimental Λ separation energy is $B_\Lambda^{\mathrm{exp}}(^9_\Lambda\mathrm{Be})=6.71\pm0.04$ MeV. The suffix "ext" stands for extrapolation.

R_C (fm)	0	6	10	14	∞
$E(^8\mathrm{Be})$	−1.260	−0.133	>0		
		+1.127	>+0.133		
			(>+1.260)		
$\varepsilon_{2\alpha}$	−0.384	1.051	1.180	1.181	$(1.181)_{\mathrm{ext}}$
		+1.435	+0.129	+0.001	-
			(+1.564)	(+1.565)	$(+1.565)_{\mathrm{ext}}$
$E(^9_\Lambda\mathrm{Be})$	−8.543	−6.922	−6.837	−6.837	$(-6.837)_{\mathrm{ext}}$
		+1.621	+0.085	+0.000	-
			(+1.706)	(+1.706)	$(+1.706)_{\mathrm{ext}}$
$B_\Lambda(^9_\Lambda\mathrm{Be})$	7.283	6.789	>6.837		
$\varepsilon_{\Lambda\alpha}$	1.390	1.228	1.260	1.261	$(+1.261)_{\mathrm{ext}}$

$$E\left({}^{9}_{\Lambda}\mathrm{Be}\right) = 21.21 - 28.09 = -6.879 \text{ MeV},$$

$$\varepsilon_{2\alpha} = 13.64 - 12.99 = 0.649 \text{ MeV},$$

$$\varepsilon_{\Lambda\alpha} = 8.264 - 7.548 = 0.715 \text{ MeV},$$

$$c_{(40)} = 0.569. \tag{31}$$

If we compare this result with Eq. (30) for the MN force, we find that the energy gain by the more attractive VN2 force is only 42 keV. This result is rather surprising, if we consider that the VN2 force gives a two-α bound state with energy $E_{2\alpha}=-245$ keV. The $\Lambda\alpha$ interaction by the SB force is also more attractive than in the MN force case due to the different choice of the h.o. width parameter ν. In other words, the ground state energy of ${}^{9}_{\Lambda}$Be is not much affected by the poor $\alpha\alpha$ and $\Lambda\alpha$ interactions, as long as we find a well-converged value by taking enough partial waves and a large number of momentum discretization points. On the other hand, the $\varepsilon_{2\alpha}$ and $\varepsilon_{\Lambda\alpha}$ values for the MN force are larger than those for the VN2 force by almost 500 keV. This may be related to the difference of ν values in the two calculations. The smaller ν value, 0.257 fm^{-2}, in the MN force calculation means more extended α-clusters than in the VN2 calculation ($\nu = 0.275$ fm^{-2}), which implies in turn that the relative wave functions in the 2α and $\Lambda\alpha$ subsystems should be more compact in the MN case. This can be confirmed by comparing the kinetic-energy contributions in $E({}^{9}_{\Lambda}\mathrm{Be})$, $\varepsilon_{2\alpha}$ and $\varepsilon_{\Lambda\alpha}$ in Eqs. (30) and (31). For example, the kinetic-energy contribution in $\varepsilon_{2\alpha}$ is 13.64 MeV in the VN2 case, while in the MN case it has a much larger value 19.46 MeV. The compactness of the $\alpha\alpha\Lambda$ relative wave function in the MN case is also reflected in the fact that $c_{(40)}$ is larger in the MN case, even though the binding energy is smaller. Comparing the result in Eq. (30) with the experimental value $E^{\mathrm{exp}}({}^{9}_{\Lambda}\mathrm{Be}) = -6.62 \pm 0.04$ MeV, we can conclude that the MN+SB combination overbinds the ${}^{9}_{\Lambda}$Be ground-state energy by 220 keV. This is partly because our SB potential is of the pure Serber type ($u=1$). If we choose $u=0.82$ for the SB force, the combination with the present MN force and $\nu=0.257$ fm^{-2} yields $E({}^{9}_{\Lambda}\mathrm{Be}) = -6.621$ MeV. In this case, the ${}^{5}_{\Lambda}$He bound-state energy is -3.105 MeV.

We list the results of various ΛN effective forces used by Hiyama *et al.* in Table VIII, when they are used in combination with the MN force for the $\alpha\alpha$ RGM kernel. The calculations are carried out with n_1-n_2-n_3=10-10-5, $R_C=10$ fm, and the partial waves up to the G-wave, to obtain the converged results with the accuracy of 1–2 keV.

Table IX lists $\alpha\alpha\Lambda$ Faddeev calculations for the 2^+ excited state, including the cut-off Coulomb force with $R_C = 14$ fm. The momentum discretization points with n_1-n_2-n_3 =10-10-5 are employed. When the partial waves are restricted to D-S or S-D, the 2^+-state energy is located above the $\alpha+{}^{5}_{\Lambda}$He threshold with the threshold energy -3.12 MeV. The listing therefore starts from the 7-channel calculation with D-P. We find that the result is almost converged with I-I and $R_C=14$ fm, within the accuracy of 1 keV. The final result for the 2^+ excited state in the MN+SB model is

TABLE VIII. $\alpha\alpha\Lambda$ Faddeev calculations for the $L^{\pi}=0^+$ ground state, including the cut-off Coulomb force with $R_C=10$ fm. The $\alpha\alpha$ RGM kernel is generated from the three-range MN force with $u = 0.946\,87$ and $\nu=0.257$ fm^{-2} for the h.o. width parameter of the α-clusters. The G-matrix based effective ΛN forces in Ref. [7] are used for the $\Lambda\alpha$ interaction, by slightly modifying the short-range repulsive part to fit the Λ separation energy $B_{\Lambda}({}^{5}_{\Lambda}\mathrm{He}) = 3.120$ MeV. Partial waves up to $\lambda_{\max}$ are included in $\alpha\alpha$-Λ channel and those up to $\ell_{1_{\max}}$ are included in the $\Lambda\alpha$-α channel. The heading $E({}^{9}_{\Lambda}\mathrm{Be})$ is the three-body ground-state energy of ${}^{9}_{\Lambda}$Be in the $\alpha\alpha\Lambda$ model, $\varepsilon_{2\alpha}$ the two-α expectation value determined self-consistently, and $\varepsilon_{\Lambda\alpha}$ the $\Lambda\alpha$ expectation value, and $c_{(40)}$ is the overlap with the shell model (40) wave function.

Force	$\lambda_{\max}$-$\ell_{1_{\max}}$	$E({}^{9}_{\Lambda}\mathrm{Be})$	$\varepsilon_{2\alpha}$	$\varepsilon_{\Lambda\alpha}$	$c_{(40)}$
NS	*S-S*	−5.580	0.909	1.136	0.606
	D-P	−6.681	1.122	1.250	0.683
	D-D	−6.736	1.133	1.255	0.686
	G-G	−6.743	1.132	1.257	0.686
ND	*S-S*	−5.734	0.764	0.774	0.579
	D-P	−7.375	1.136	0.838	0.693
	D-D	−7.478	1.159	0.842	0.697
	G-G	−7.483	1.157	0.843	0.697
NF	*S-S*	−5.682	0.802	0.882	0.587
	D-P	−6.839	1.009	0.942	0.666
	D-D	−6.901	1.021	0.944	0.669
	G-G	−6.906	1.020	0.944	0.669
JA	*S-S*	−5.620	0.862	1.030	0.599
	D-P	−6.622	1.022	1.112	0.667
	D-D	−6.672	1.031	1.114	0.669
	G-G	−6.677	1.031	1.115	0.669
JB	*S-S*	−5.566	0.915	1.154	0.606
	D-P	−6.431	1.027	1.253	0.664
	D-D	−6.469	1.034	1.255	0.666
	G-G	−6.475	1.033	1.256	0.666

$$E = 29.47 - 33.40 = -3.926 \text{ MeV},$$

$$\varepsilon_{2\alpha} = 21.55 - 17.54 = 4.013 \text{ MeV},$$

$$\varepsilon_{\Lambda\alpha} = 9.481 - 7.930 = 1.551 \text{ MeV},$$

$$c_{(40)} = 0.645. \tag{32}$$

If we compare Eqs. (30) and (32), we find that the 3 MeV excitation energy of the 2^+ state mainly comes from an increase of the two-α kinetic energy (2 MeV) and from the two-α potential energy (1 MeV). This clearly shows the rotational nature of the ground 0^+ and excited 2^+ states, com-

TABLE IX. Same as Table VIII, but for the $L^\pi = 2^+$ excited state with $R_C = 14$ fm.

Force	$\lambda_{\max}$-$\ell_{1_{\max}}$	$E(^9_\Lambda\mathrm{Be})$	$\varepsilon_{2\alpha}$	$\varepsilon_{\Lambda\alpha}$	$c_{(40)}$
	D-P	−3.797	3.987	1.528	0.643
SB	*D-D*	−3.874	4.014	1.536	0.645
	G-G	−3.926	4.013	1.550	0.645
	I-I	−3.926	4.013	1.551	0.645
	D-P	−3.700	3.920	1.518	0.639
NS	*D-D*	−3.772	3.946	1.525	0.641
	G-G	−3.831	3.942	1.544	0.641
	I-I	−3.831	3.943	1.544	0.641
	D-P	−4.377	4.027	1.130	0.648
ND	*D-D*	−4.518	4.071	1.134	0.651
	G-G	−4.553	4.066	1.137	0.651
	I-I	−4.553	4.067	1.138	0.651
	D-P	−3.853	3.825	1.223	0.637
NF	*D-D*	−3.938	3.851	1.226	0.639
	G-G	−3.981	3.849	1.236	0.639
	I-I	−3.981	3.849	1.236	0.639
	D-P	−3.645	3.805	1.380	0.635
JA	*D-D*	−3.710	3.827	1.385	0.637
	G-G	−3.762	3.825	1.401	0.637
	I-I	−3.762	3.826	1.402	0.637
	D-P	−3.460	3.775	1.507	0.632
JB	*D-D*	−3.510	3.792	1.511	0.633
	G-G	−3.568	3.793	1.535	0.634
	I-I	−3.568	3.794	1.535	0.634

posed of the two-α cluster structure with a weakly coupled Λ.

Table X summarizes the present results with the MN force for the $\alpha\alpha$ RGM kernel. The SB result shows the overbinding of the $^9_\Lambda$Be ground-state energy by about 220 keV and too small excitation energy of the 2^+ excited state by about 130 keV. Table X also shows a comparison with the results by Hiyama *et al.* [7] for the *G*-matrix based effective ΛN forces. We find that their results are a little lower than our results by about 70–90 keV. Since their calculation is a variational calculation using a smaller model space than ours, this is not a convergence problem of the variational calculation. A possible reason is the difference between OCM and RGM in the $\alpha\alpha$ part. They used $\alpha\alpha$ OCM, while ours is $\alpha\alpha$ RGM. The OCM usually gives more attractive results than the RGM. In fact, it is well known that 3α OCM usually gives a larger binding energy than the 3α RGM for the ground state of the 3α system [59]. A small difference in the exchange term of the $\Lambda\alpha$ folding potential may also contribute to this difference.

TABLE X. Summary of the ground-state energy $E_{\mathrm{gr}}(0^+)$ and the 2^+ excitation energy $E_{\mathrm{x}}(2^+)$ in MeV, calculated by solving the Faddeev equation for the $\alpha\alpha\Lambda$ system in the *LS* coupling scheme. The $\alpha\alpha$ RGM kernel is generated from the three-range MN force with $u = 0.946\,87$ and $\nu = 0.257$ fm^{-2} for the h.o. width parameter of the α-clusters.

$V_{\Lambda N}$	$E_{\mathrm{gr}}(0^+)$ (MeV)		$E_{\mathrm{x}}(2^+)$ (MeV)
	Present	Ref. [7]	
SB	−6.837	-	2.911
NS	−6.742	−6.81	2.912
ND	−7.483	−7.57	2.930
NF	−6.906	−7.00	2.925
JA	−6.677	−6.76	2.915
JB	−6.474	−6.55	2.907
Expt	-6.62 ± 0.04		3.024(3)
[30,31]			3.067(3)

If we arrange the effective ΛN forces in Table X in the order of more attractive nature, we find

$$\mathrm{ND}(-7.483) > \mathrm{NF}(-6.906) > \mathrm{SB}(-6.837) > \mathrm{NS}(-6.742) > \mathrm{JA}(-6.677) > \mathrm{JB}(-6.474). \quad (33)$$

The experimental value -6.62 ± 0.04 MeV is located between JA and JB. However, this does not mean that the Jülich potentials JA and JB are the most correct ΛN interactions. It is well known that the spin-spin central terms of these Jülich potentials are completely wrong and that they fail to reproduce the observed energy spectrum of the $^4_\Lambda$H and $^4_\Lambda$He systems [60]. As for the 2^+ excitation energy, all the results in Table X are between 2.91 and 2.93 MeV. They are too small by 110–130 keV with respect to the average value 3.04 MeV of the two resonances recently observed by γ-ray spectroscopy [30,31]. Since the experimental error bars are at most ±40 keV even in the (K,π) reaction [26], this is a meaningful disagreement. It would be interesting to examine the ℓs splitting of the $5/2^+$-$3/2^+$ states, by introducing a small ΛN spin-orbit force predicted by our quark-model interaction.

In order to show that the present $\alpha\alpha$ RGM kernel gives a better result than simple $\alpha\alpha$ potentials, we show in Table XI some results of $\alpha\alpha\Lambda$ Faddeev calculations using the Ali-Bodmer potential, ABd [12], and the Buck, Friedrich, and Wheatley potential, BFW [11]. In these cases, there needs to be no self-consistent procedure to determine $\varepsilon_{2\alpha}$. We only use the SB potential for the $\Lambda\alpha$ interaction, since results with other effective ΛN forces are easily evaluated from the above discussion in the case of the $\alpha\alpha$ RGM kernel. In these α-particle models, we customarily use $\hbar^2/M_\alpha = 10.4465$ MeV fm^2 and $e^2 = 1.44$ MeV fm. The momentum discretization points with n_1-n_2-n_3 = 15-10-5 are employed.

TABLE XI. $\alpha\alpha\Lambda$ Faddeev calculations for the $L^\pi=0^+$ ground state by the Ali-Bodmer (ABd) [12] and Buck, Friedrich, and Wheatley (BFW) [11] $\alpha\alpha$ potentials. The SB ΛN force is used for the $\Lambda\alpha$ interaction. The cut-off Coulomb force is included at the nucleon level with $R_C=10$ fm. The h.o. width parameters of the α-clusters are assumed to be $\nu=0.271\,27$ fm^{-2} (ABd) and $\nu=0.257$ fm^{-2} (BFW). The parameters $\hbar^2/M_\alpha=10.4465$ MeV fm^2 and $e^2=1.44$ MeV fm are used. Partial waves up to $\lambda_{\max}$ are included in the $\alpha\alpha$-Λ channel and those up to $\ell_{1\max}$ in the $\Lambda\alpha$-α channel. The momentum discretization points with n_1-n_2-n_3 =15-10-5 are employed. The $\Lambda\alpha$ bound-state energy $E(^5_\Lambda\mathrm{He})$ for the SB ΛN force is given in the first column.

$E(^5_\Lambda\mathrm{He})$	$\lambda_{\max}$ -$\ell_{1_{\max}}$	$E(^9_\Lambda\mathrm{Be})$	$\varepsilon_{2\alpha}$	$\varepsilon_{\Lambda\alpha}$	$c_{(40)}$
		ABd+SB			
	S-S	−6.409	0.970	−0.503	0.466
	D-P	−7.091	1.013	−0.532	0.497
−3.183	*D-D*	−7.147	1.013	−0.526	0.499
	G-G	−7.153	1.018	−0.518	0.498
	I-I	−7.153	1.018	−0.517	0.498
		BFW+SB			
	S-S	−5.544	0.861	1.776	0.630
	D-P	−6.971	1.147	1.973	0.724
−3.066	*D-D*	−7.038	1.155	1.979	0.728
	G-G	−7.043	1.161	1.979	0.728
	I-I	−7.043	1.161	1.980	0.728

For the $\alpha\alpha$ Coulomb potential, the folding potential of the cut-off Coulomb force with the $(0s)^4$ shell-model wave function is used with $R_C=10$ fm. The h.o. width parameter of the $(0s)^4$ α-cluster for this Gaussian folding is $\nu=0.271\,27$ fm^{-2} in the ABd case and $\nu=0.257$ fm^{-2} in the BFW case. In the ABd case, this ν value corresponds to the Coulomb-force parameter $\beta=\sqrt{3}/(2\times1.44)=0.6014$ fm^{-1} and the α rms radius, $r_\alpha=(3/4\sqrt{\nu})=1.44$ fm. Since this ν value is also used for the α-cluster folding for the ΛN potential, the $\Lambda\alpha$ bound-state energy $E(^5_\Lambda\mathrm{He})$ is a little shifted from the fitted experimental value −3.12 MeV. [The different $\hbar^2/M_N$ value also affects this difference.] Since the energy change is only about 0.06 MeV, we do not readjust the potential parameters of the ΛN force. In the BFW case, the ν value, 0.257 fm^{-2}, corresponds to $\beta=\sqrt{4\nu/3}=0.585\,38$ fm^{-1} and the rms radius of the α-cluster, $r_\alpha=\sqrt{3}/(2\beta)=1.48$ fm. In this case the difference of the ΛN bound-state energy, 0.054 MeV, from −3.12 MeV is solely from the different $\hbar^2/M_N$ value. The bound-state solutions of the BFW potential are used for the pairwise Pauli-forbidden states. The elimination of the Pauli-forbidden components from the three-body total wave function is always inspected by calculating their squared norm, which is of the order of 10^{-13}.

We find that the $\alpha\alpha\Lambda$ ground-state energy by the ABd potential is lower than the result of the MN force in Eq. (30) by 0.3 MeV. Note that even in this case the energy gain from the higher partial waves than the *S* wave is appreciable, i.e., 0.7 MeV. This implies that the *S*-wave assumption adopted by Filikhin and Gal [34] is not valid. They used a little different version of the Ali-Bodmer potential (type (a) with 125 MeV modified by 120 MeV) and obtained $E(^9_\Lambda\mathrm{Be})=-6.55$ MeV in the *S*-wave approximation. We expect an energy gain of about 0.7 MeV from the higher partial waves and their result is overbound, in comparison with the experimental value, -6.62 ± 0.04 MeV. In Table XI, we find that the BFW potential gives a better result than the Ali-Bodmer force, but the energy is still lower than in the MN force case by 0.2 MeV. In this case we find that the effect of partial waves higher than the *S* wave is quite appreciable, i.e., −1.5 MeV. This is of course due to the inner oscillation of the relative wave function between the two α-clusters in the $\alpha\alpha\Lambda$ ground state. The shell-model like (40) components are about 0.7 in amplitude, which is appreciably larger than $c_{(40)}\sim0.5$ in the Ali-Bodmer case.

IV. SUMMARY

The three-cluster Faddeev formalism using two-cluster resonating-group method (RGM) kernels opens a way to solve few-baryon systems interacting via quark-model baryon-baryon interactions without spoiling essential features of the RGM kernel, i.e., the non-locality, the energy dependence proportional to the exchange normalization kernel, and the existence of pairwise Pauli-forbidden states in some specific channels. In this paper, we have applied this formalism to three-cluster systems involving α-clusters, i.e., the 3α and $\alpha\alpha\Lambda$ systems. These systems involve all of the above three features for the microscopic interactions between composite particles. In particular, the $\alpha\alpha$ interaction is a prototype of composite-particle interactions, in which the fully microscopic RGM calculation is easy and very successful. It, however, involves a somewhat complex kernel structure composed of three non-trivial Pauli-forbidden states, and the energy-dependence of the interaction is rather strong in the Pauli-allowed model space. In the present Faddeev formulation, the Pauli-forbidden components between pairwise clusters are completely eliminated from the total wave function of the three clusters. This can be achieved by introducing a special type of RGM $\widetilde{T}$-matrix calculated from the two-cluster RGM kernel, which satisfies the *T*-matrix version of the orthogonality conditions to the relative motion between two clusters. The on-shell and half off-shell properties of the $\widetilde{T}$-matrix are just the same as those of the ordinary *T*-matrix. This RGM $\widetilde{T}$-matrix involves a relative energy of two clusters as a parameter, which is determined self-consistently by calculating the expectation value of the two-cluster Hamiltonian with respect to the total wave function resulting from the Faddeev equation. The Faddeev equation using $\widetilde{T}$-matrices is equivalent to the pairwise orthogonality condition model (OCM) of three-cluster systems, interacting via two-cluster RGM kernels. A nice point of this formalism is that the underlying nucleon-nucleon (*NN*) and hyperon-nucleon (*YN*) interactions are more directly related to the structure of three-cluster systems than in the models assuming simple two-cluster potentials.

We have first applied the present formalism to the ground state of the 3α system by using three different types of effective *NN* forces, the two-range Volkov forces, No.1 (VN1) and No. 2 (VN2), and the three-range Minnesota (MN) force. The three-range MN force reproduces the *S*-, *D*- and *G*-wave $\alpha\alpha$ phase shifts quite well in the simple $(0s)^4$-model of the α clusters. The comparison with the 3α RGM calculation has shown that the present three-cluster formalism using only the $\alpha\alpha$ RGM kernel gives a good approximation to the microscopic 3α model. The difference of the ground-state energies predicted by these two models is less than 2 MeV. The effect of the antisymmetrization among three α-clusters, which is neglected in our formulation, is attractive and is not so large, as long as the Pauli-allowed model space of the 3α system is properly treated. It is also shown that the three-range MN force gives a lower ground-state energy than the two-range VN1 and VN2 forces, resulting in a somewhat large overbinding of 2–4 MeV, if the 3α ground-state energy is measured from the 3α threshold.

The application to the ${}^{9}_{\Lambda}$Be system has proved that our three-cluster formalism is soundly extended to the systems with two identical clusters, in addition to the systems of three identical clusters like the 3α system and the triton system. Here we have introduced a new effective ΛN force, called the SB force, which is made from the quark-model predictions of the ΛN phase shifts by using an inversion method based on supersymmetric quantum mechanics [42]. The SB force consists of two simple two-range Gaussian potentials which reproduce the low-energy behavior of the ${}^1S_0$ and ${}^3S_1$ ΛN phase shifts predicted by ΛN-ΣN coupled-channel RGM calculations using the model fss2 [46]. Since any central and single-channel effective ΛN force leads to the well-known overbinding problem of ${}^{5}_{\Lambda}$He by about 2 MeV [50], the attractive part of the ${}^3S_1$ ΛN potential is reduced by about 10% to reproduce the empirical Λ-separation energy, $B_{\Lambda}^{\rm exp}({}^{5}_{\Lambda}{\rm He}) = 3.12 \pm 0.02$ MeV. The odd-state ΛN force is assumed to be zero (pure Serber type). In addition to this SB force, we have also used the effective ΛN forces in Ref. [7] for comparison. The $\Lambda\alpha$ interactions are generated from these ΛN effective forces by the folding procedure with respect to the $(0s)^4$ h.o. wave function of the α clusters.

In the $\alpha\alpha\Lambda$ Faddeev calculation, sufficient partial waves up to $\lambda_{\rm Max} = \ell_{1{\rm Max}} = 6$ are included both in the $\alpha\alpha$ and $\Lambda\alpha$ pairs since the relative wave functions between two α-clusters are oscillating at least in the relative *S*- and *D*-waves. The detailed analysis shows that the partial waves up to the *D*-wave are sufficient if we do not mind a 10 keV inaccuracy. If we wish to obtain a 1 keV accuracy, we need to take into account at least up to the *G*-wave. This implies that the partial wave truncation is very efficient even in the present Faddeev formalism. The energy gain due to partial waves higher than the *S*-wave is about 1 MeV for the VN2 force and 1.2 MeV for the MN force, when these $\alpha\alpha$ interactions are used in combination with the SB force for the $\Lambda\alpha$ interaction. The Coulomb effect between the two α-clusters is included by a cut-off Coulomb force at the nucleon level. The cut-off radius, $R_C = 10-14$ fm seems to be sufficient for a 1–2 keV accuracy. In the present formalism, the structure change of two α-clusters inside ${}^{9}_{\Lambda}$Be is clearly identified by calculating the kinetic-energy contribution in the two-α expectation value $\varepsilon_{2\alpha}$. The comparison of the Coulomb contributions in the $\alpha\alpha$ bound state, $\varepsilon_{2\alpha}$ and the ${}^{9}_{\Lambda}$Be ground state with respect to the change of R_C is very useful to measure the compactness of the two-α configurations in various environments. It is confirmed that the 0^+ ground state and the 2^+ exited state of ${}^{9}_{\Lambda}$Be are well described by the contracted two-α cluster structure with a weakly coupled Λ-particle in the dominant *S*-wave component. In the present calculation using only central forces, the three-range MN force and the SB potential with the pure-Serber character can reproduce the ground-state and excitation energies of ${}^{9}_{\Lambda}$Be within an accuracy of 100–200 keV. The results in Ref. [7] based on the OCM framework are also confirmed within 100 keV accuracy. On the other hand, the simple α-particle model using the Ali-Bodmer $\alpha\alpha$ potential, ABd [12], and the OCM using the deep Buck, Friedrich, and Wheatley $\alpha\alpha$ potential, BFW [11], with bound-state Pauli-forbidden states give an overbinding of the ${}^{9}_{\Lambda}$Be ground state by 530 and 420 keV, respectively, when the SB force is used for the $\Lambda\alpha$ interaction. Although these energies are rather similar, the effect of partial waves higher than the *S*-wave is very different, i.e., 0.7 MeV in the Ali-Bodmer case and 1.5 MeV in the BFW case. It is natural that the $\alpha\alpha$ interactions which yield an oscillatory behavior of the $\alpha\alpha$ relative wave functions, like our RGM kernel and the BFW potential, need more partial waves with a larger energy gain.

There are still many problems left for future studies. First of all, the readjustment of the ${}^3S$ attractive part of the SB ΛN potential is unsatisfactory from the viewpoint of using the fundamental baryon-baryon interactions. The Brueckner rearrangement effect in ${}^{5}_{\Lambda}$He is fairly large even for the rather stable α-cluster [50]. In this sense, there is still no consistent description of the *s*-shell and *p*-shell hypernuclei even at the level of using effective baryon-baryon interactions. A microscopic description of the $\Lambda\alpha$ interaction may need a more detailed analysis based on the *G*-matrix theory, for which the folding formula given in Appendix B is very useful. In order to describe the ${}^{9}_{\Lambda}$Be excited states realistically, we need to introduce the $\Lambda\alpha$ spin-orbit force and solve the Faddeev equation in the *jj*-coupling scheme. The recent γ-ray spectroscopy experiment [30,31] indicates a very small spin-orbit splitting for the possible $5/2^+$ and $3/2^+$ resonances. It is interesting to examine the *LS* components of the quark-model ΛN interaction, in which the antisymmetric *LS* interaction ($LS^{(-)}$) is by about a factor two larger than in the Nijmegen models. We expect a large cancellation between the ordinary *LS* interaction and this $LS^{(-)}$ interaction. An interesting application of the present Faddeev formalism and the $\Lambda\alpha$ *T*-matrix derived in this study is to the recent Nagara event [61] for ${}^{6}_{\Lambda\Lambda}$He. For the $\Lambda\Lambda$ interaction, we can use the coupled-channel $\Lambda\Lambda$-ΞN-$\Sigma\Sigma$ $\widetilde{T}$-matrix of the quark-model interaction, fss2. A preliminary result [41] shows that fss2 is at present the only model which can reproduce an appropriate strength of the $\Lambda\Lambda$ interaction, $\Delta B_{\Lambda\Lambda}^{\rm exp} = 1.01 \pm 0.20$ MeV, deduced from the Nagara event. In a separate paper [22], we have also reported another application of the present three-cluster Faddeev formalism to the hypertriton system, in which the quark-model *NN* and *YN* interactions are explicitly

used in the ΛNN and ΣNN coupled-channel Faddeev formalism. In this system, a complete Pauli-forbidden state at the quark level exists in the ΛN-ΣN subsystem.

ACKNOWLEDGMENTS

This work was supported by Grants-in-Aid for Scientific Research (C) from the Japan Society for the Promotion of Science (JSPS) (Nos. 15540270, 15540284, and 15540292). Y.F. wishes to thank the FNRS foundation of Belgium for making his visit to the Free University of Brussels possible during the summer, 2002.

APPENDIX A: REARRANGEMENT FACTORS OF THREE-CLUSTER SYSTEMS WITH TWO IDENTICAL PARTICLES

In this Appendix, we give a brief comment on the definition of the rearrangement factors in the Dirac notation for general three-body systems with two identical particles or clusters. The incorporation of spin-isospin degrees of freedom is essential for further applications to the hypertriton system [22] and the $\Lambda\Lambda\alpha$ system [41]. When one uses the Dirac notation, it is important to fix a coordinate system of the representation. We choose the standard system of the Jacobi coordinates with $\gamma=3$, and introduce the Jacobi coordinates in the momentum space, $\boldsymbol{p}=\boldsymbol{p}_3$ and $\boldsymbol{q}=\boldsymbol{q}_3$. The other Jacobi coordinates $\boldsymbol{p}_1$, $\boldsymbol{q}_1$, etc., are similarly defined. For an arbitrary function $\psi(\boldsymbol{p},\boldsymbol{q};123)$ in $\gamma=3$, the effect of the cyclic permutation $P_{(123)}$ of the symmetric group S_3 is

$$P_{(123)}\psi(\boldsymbol{p}_2,\boldsymbol{q}_2;312)=P_{(123)}{}^2\psi(\boldsymbol{p}_1,\boldsymbol{q}_1;231)=\psi(\boldsymbol{p}_3,\boldsymbol{q}_3;123), \tag{A1}$$

where 123 in $\psi(\boldsymbol{p},\boldsymbol{q};123)$ stands for the spin-isospin variables. For the transposition $P_{(12)}$, Eq. (1) yields

$$P_{(12)}\psi(\boldsymbol{p}_3,\boldsymbol{q}_3;123)=\psi(-\boldsymbol{p}_3,\boldsymbol{q}_3;213),$$

$$P_{(12)}\psi(\boldsymbol{p}_1,\boldsymbol{q}_1;231)=\psi(-\boldsymbol{p}_2,\boldsymbol{q}_2;132),$$

$$P_{(12)}\psi(\boldsymbol{p}_2,\boldsymbol{q}_2;312)=\psi(-\boldsymbol{p}_1,\boldsymbol{q}_1;321). \tag{A2}$$

Note that the momentum suffix α in $\boldsymbol{p}_\alpha$, $\boldsymbol{q}_\alpha$, and the sign of $\boldsymbol{p}_\alpha$, etc., are uniquely specified by the sequence of 123. For example, $\langle\hat{\boldsymbol{p}}_2,\hat{\boldsymbol{q}}_2|\beta\rangle$ in Eq. (4) actually implies $\langle\hat{\boldsymbol{p}}_2,\hat{\boldsymbol{q}}_2;312|\beta\rangle$. In the following, we always use an abbreviated notation, $\psi=\psi(\boldsymbol{p}_3,\boldsymbol{q}_3;123)$, in the standard coordinate system $\gamma=3$. The total wave function, $\Psi(\boldsymbol{q}_3,\boldsymbol{q}_3;123)$, in Eq. (2) is then compactly expressed as

$$\Psi=\psi\pm P_{(12)}P_{(123)}{}^2\varphi+P_{(123)}{}^2\varphi. \tag{A3}$$

If we write the Faddeev equation in terms of ψ and φ, it reads

$$\psi=G_0\widetilde{T}(1\pm P_{(12)})P_{(123)}{}^2\varphi,$$

$$\varphi=G_0T[P_{(123)}\psi\pm P_{(23)}\varphi], \tag{A4}$$

with $\widetilde{T}=T_{12}$ and $T=P_{(123)}T_{13}P_{(123)}{}^{-1}$, where T_{12} and T_{13} are the two-body T-matrices in the three-body space.

The definition of the rearrangement factors in the Dirac notation is based on the assumption

$$\begin{aligned}\langle\boldsymbol{p}_3,\boldsymbol{q}_3;123|P_{(123)}{}^2\varphi\rangle&=P_{(123)}{}^2\varphi(\boldsymbol{p}_3,\boldsymbol{q}_3;123)=\varphi(\boldsymbol{p}_2,\boldsymbol{q}_2;312)\\&=\int d\mathbf{p}'d\mathbf{q}'\,\delta(\boldsymbol{p}'-\boldsymbol{p}_2)\delta(\boldsymbol{q}'-\boldsymbol{q}_2)\\&\quad\times P_{(123)}^{(\sigma\tau)\,2}\varphi(\boldsymbol{p}',\boldsymbol{q}';123),\end{aligned} \tag{A5}$$

where the function $\varphi(\boldsymbol{p}_3,\boldsymbol{q}_3;123)$ is φ in Eq. (A3) and $P_{(123)}^{(\sigma\tau)}$ operates only on the spin-isospin variables of $\varphi(\boldsymbol{p}',\boldsymbol{q}';123)$. With this φ in the $\beta=2$ channel in mind, the standard procedure of the partial wave decomposition gives the following definition for the first-type rearrangement factor $g_{\gamma\beta}(q,q';x)$:

$$\begin{aligned}\langle p,q,\gamma|P_{(123)}{}^2|p',q',\beta\rangle_{3-2}&=\frac{1}{2}\int_{-1}^{1}dx\frac{\delta(p-p_1)}{p^{\lambda+2}}\frac{\delta(p'-p_2)}{p'^{\ell_1+2}}g_{\gamma\beta}(q,q';x)=\sum_{123}\int d\hat{\boldsymbol{p}}d\hat{\boldsymbol{q}}d\hat{\boldsymbol{p}}'d\hat{\boldsymbol{q}}'\langle\gamma|\hat{\boldsymbol{p}},\hat{\boldsymbol{q}};123\rangle\\&\quad\times\delta\left(\boldsymbol{p}+\boldsymbol{q}'+\frac{m_2}{m_2+m_1}\boldsymbol{q}\right)\delta\left(\boldsymbol{p}'-\boldsymbol{q}-\frac{m_3}{m_3+m_1}\boldsymbol{q}'\right)P_{(123)}^{(\sigma\tau)\,2}\langle\hat{\boldsymbol{p}}',\hat{\boldsymbol{q}}';123|\beta\rangle.\end{aligned} \tag{A6}$$

Here, p_1 and p_2 are given in Eq. (5c) with a general mass factor, $\zeta=(4m_3/m_1)$. With this mass modification, Eq. (6) is valid with a more complete reduced rearrangement factor

$$g^{\lambda_1\lambda_1' k}_{\gamma\beta} = \begin{cases} (-1)^{\lambda} G^{\lambda_1\lambda_1' kL}_{(\lambda\ell),(\ell_1\ell_2)} \langle STT_z;\gamma \| P^{(\sigma\tau)\,2}_{(123)} \| STT_z;\beta\rangle & (LS\text{-coupling}) \\ (-1)^{\lambda} \sum_{LS} \begin{bmatrix} \lambda & s_1 & I \\ \ell & s_2 & j \\ L & S & J \end{bmatrix} \begin{bmatrix} \ell_1 & s_1' & j_1 \\ \ell_2 & s_2' & j_2 \\ L & S & J \end{bmatrix} G^{\lambda_1\lambda_1' kL}_{(\lambda\ell),(\ell_1\ell_2)} \langle STT_z;\gamma \| P^{(\sigma\tau)\,2}_{(123)} \| STT_z;\beta\rangle & (jj\text{-coupling}). \end{cases} \tag{A7}$$

Here the square bracket implies the unitary form of the $9j$ coefficients and the quantum numbers are specified by

$$\begin{cases} |\gamma\rangle = |[(\lambda\ell)LS]JJ_z;TT_z\rangle, \quad |\beta\rangle = |[(\ell_1\ell_2)LS]JJ_z;TT_z\rangle & (LS\text{-coupling}), \\ |\gamma\rangle = |[(\lambda s_1)I(\ell s_2)j]JJ_z;TT_z\rangle, \quad |\beta\rangle = |[(\ell_1 s_1')j_1(\ell_2 s_2')j_2]JJ_z;TT_z\rangle & (jj\text{-coupling}). \end{cases} \tag{A8}$$

The angular-momentum factors $G^{\lambda_1\lambda_1' kL}_{(\lambda\ell),(\ell_1\ell_2)}$ with $\lambda_1 = 0 \sim \lambda$, $\lambda_1' = 0 \sim \ell_1$ are given by

$$G^{\lambda_1\lambda_1' kL}_{(\lambda\ell),(\ell_1\ell_2)} = G^{\lambda_1'\lambda_1 kL}_{(\ell_1\ell_2),(\lambda\ell)} = \left[\frac{(2\lambda+1)!\,(2\ell_1+1)!}{(2\lambda_1)!\,(2\lambda_2)!\,(2\lambda_1')!\,(2\lambda_2')!} \right]^{1/2} \hat{\lambda}\hat{\ell}\hat{\ell}_1\hat{\ell}_2 \sum_{f,f'} \langle \lambda_2 0 \ell 0 | f 0\rangle \langle \lambda_2' 0 \ell_2 0 | f' 0\rangle \langle k 0 \lambda_1 0 | f' 0\rangle \langle k 0 \lambda_1' 0 | f 0\rangle$$
$$\times \begin{Bmatrix} f & L & \lambda_1 \\ \lambda & \lambda_2 & \ell \end{Bmatrix} \begin{Bmatrix} f' & L & \lambda_1' \\ \ell_1 & \lambda_2' & \ell_2 \end{Bmatrix} \begin{Bmatrix} \lambda_1' & f' & L \\ \lambda_1 & f & k \end{Bmatrix}, \tag{A9}$$

where $\hat{\lambda} = \sqrt{2\lambda+1}$, etc. and $\lambda_2 = \lambda - \lambda_1$, $\lambda_2' = \ell_1 - \lambda_1'$. In the spin-isospin reduced matrix elements of Eq. (A7), the permutation operator $P^{(\sigma\tau)^2}_{(123)}$ does not change the total spin and isospin values, S and TT_z.

The other types of rearrangement factors are obtained in a similar way. First, the symmetry of the matrix elements yields

$$\langle p,q,\beta|P_{(123)}|p',q',\gamma\rangle_{2-3} = \langle p',q',\gamma|P_{(123)^2}|p,q,\beta\rangle_{3-2}. \tag{A10}$$

The rearrangement factor for the matrix element $\langle\varphi|P_{(23)}|\varphi\rangle$ needs a little care, since the mass assignment of the three particles is made in the standard Jacobi coordinates $\gamma = 3$. We first use $P_{(23)} = P_{(123)}P_{(12)}P_{(123)}{}^{-1}$ and write the matrix element as

$$\langle\varphi|P_{(23)}|\varphi\rangle = \sum_{123} \int d\boldsymbol{p}_3 d\boldsymbol{q}_3 \varphi^*(\boldsymbol{p}_2,\boldsymbol{q}_2;312)\varphi(-\boldsymbol{p}_1,\boldsymbol{q}_1;321). \tag{A11}$$

The corresponding rearrangement factor in the Dirac notation is given by

$$\begin{aligned} &\langle p,q,\beta|P_{(23)}|p',q',\beta'\rangle_{2-1} \\ &= \sum_{123} \int d\hat{\boldsymbol{p}} d\hat{\boldsymbol{q}} d\hat{\boldsymbol{p}}' d\hat{\boldsymbol{q}}' \langle\beta|\hat{\boldsymbol{p}},\hat{\boldsymbol{q}};123\rangle \\ &\quad \times \delta\left(\boldsymbol{p} + \boldsymbol{q}' + \frac{m_1}{m_1+m_3}\boldsymbol{q}\right) \delta\left(\boldsymbol{p}' + \boldsymbol{q} + \frac{m_2}{m_2+m_3}\boldsymbol{q}'\right) \\ &\quad \times P^{(\sigma\tau)}_{(23)} \langle\hat{\boldsymbol{p}}',\hat{\boldsymbol{q}}';123|\beta'\rangle, \end{aligned} \tag{A12}$$

from which the results in Eqs. (8) and (9) are easily obtained. Note that the rearrangement factor Eq. (A12) is symmetric with respect to the interchange between p, q, β and p', q', β', since $m_1 = m_2$.

APPENDIX B: A USEFUL FORMULA FOR THE $\Lambda\alpha$ BORN KERNEL

The general procedure to calculate Born kernels of the s-shell clusters, developed in Ref. [62], can also be used to calculate the $\Lambda\alpha$ Born kernel

$$V(\boldsymbol{q}_f,\boldsymbol{q}_i) = \langle e^{i\boldsymbol{q}_f\boldsymbol{r}}|V|e^{i\boldsymbol{q}_i\boldsymbol{r}}\rangle = \langle e^{i\boldsymbol{q}_f\boldsymbol{r}}\xi_\Lambda\phi_\alpha|\sum_{j=2}^{5} v_{1j}|e^{i\boldsymbol{q}_i\boldsymbol{r}}\xi_\Lambda\phi_\alpha\rangle, \tag{B1}$$

where ϕ_α is the internal wave function of the α cluster, ξ_Λ is the spin wave function of the Λ particle and v_{1j} is an effective ΛN interaction. The essential part of this method lies in the correct treatment of the c.m. motion which is handled by the procedure given in Ref. [63]. This method makes it possible to deal with the most general form of the ΛN interaction with non-static effects like the G-matrix ΛN interaction. In this method, $V(\boldsymbol{q}_f,\boldsymbol{q}_i)$ in Eq. (B1) is calculated from an integral form of the GCM kernel through

$$\begin{aligned} V(\boldsymbol{q}_f,\boldsymbol{q}_i) &= \langle \delta(\boldsymbol{X}_G) e^{i\boldsymbol{q}_f\boldsymbol{r}}\xi_\Lambda\phi_\alpha|\sum_{j=2}^{5} v_{1j}|1\cdot e^{i\boldsymbol{q}_i\boldsymbol{r}}\xi_\Lambda\phi_\alpha\rangle \\ &= \left(\frac{\gamma}{2\pi}\right)^{3/2} e^{(1/4\gamma)(\boldsymbol{q}_f{}^2+\boldsymbol{q}_i{}^2)} \int d\boldsymbol{a} d\boldsymbol{b} e^{-i\boldsymbol{q}_f\cdot\boldsymbol{a}+i\boldsymbol{q}_i\cdot\boldsymbol{b}} G(\boldsymbol{a},\boldsymbol{b}), \end{aligned} \tag{B2}$$

with

$$G(\boldsymbol{a},\boldsymbol{b}) = \left(\frac{\gamma_G}{2\pi}\right)^{3/2} \int d\boldsymbol{R}\, \langle \psi_\Lambda(\boldsymbol{a})\psi_\alpha(0)| \times \sum_{j=2}^{5} v_{1j} |\psi_\Lambda(\boldsymbol{R}+\boldsymbol{b})\psi_\alpha(\boldsymbol{R})\rangle. \quad \text{(B3)}$$

Here, $\gamma_G=(4+\zeta)\nu$, $\gamma=4\zeta\nu/(4+\zeta)$ with $\zeta=M_\Lambda/M_N$, and $\psi_\Lambda(\boldsymbol{R})$ and $\psi_\alpha(\boldsymbol{R})$ are the h.o. shell model wave functions of Λ and α, centered at $\boldsymbol{R}$, with the width parameters $\zeta\nu$ and ν, respectively. First we calculate spatial integrals for the spatial part u in $v_{1j}=u_{1j}\omega_{1j}$. These four integrals with $j=2-5$ are all equal because of the antisymmetric property of the α cluster. We need to calculate spatial integrals for $u=u(\boldsymbol{x}_1-\boldsymbol{x}_2)$ and $u=u(\boldsymbol{x}_1-\boldsymbol{x}_2)P_r$, which we call the direct term and the exchange term, respectively. It is important to note that the space exchange operator, P_r, operates only on the single-particle coordinates $\boldsymbol{x}_1$ and $\boldsymbol{x}_2$, and *does not* exchange the Λ and N masses. The procedure to interchange these masses M_Λ and M_N simultaneously like in Ref. [7] leads to an erroneous expression [see Eq. (A.1) of [7]], which is apparently wrong since the RGM kernel $\langle\delta(\boldsymbol{r}-\boldsymbol{a})\xi_\Lambda\phi_\alpha|\Sigma_{j=2}^{5}v_{1j}|\delta(\boldsymbol{r}-\boldsymbol{b})\xi_\Lambda\phi_\alpha\rangle$ should not involve the mass dependence. The correct expression is the one in which one sets $M_N=M_\Lambda$ in their Eq. (A.1) [see Eq. (B8) below]. The most general form of the two-body ΛN matrix elements for the translationally invariant u is parametrized as

$$\langle \boldsymbol{p}_1\boldsymbol{p}_2|u|\boldsymbol{p}_1{}'\boldsymbol{p}_2{}'\rangle = \frac{1}{(2\pi)^3}\delta(\boldsymbol{P}-\boldsymbol{P}')u(\boldsymbol{k}',\boldsymbol{q}';\boldsymbol{P}), \quad \text{(B4)}$$

with $\boldsymbol{p}=(\boldsymbol{p}_1-\zeta\boldsymbol{p}_2)/(\zeta+1)$, $\boldsymbol{P}=\boldsymbol{p}_1+\boldsymbol{p}_2$ (also $\boldsymbol{p}'$, $\boldsymbol{P}'$ for $\boldsymbol{p}_1'$, $\boldsymbol{p}_2'$), and $\boldsymbol{k}'=\boldsymbol{p}-\boldsymbol{p}'$, $\boldsymbol{q}'=(\boldsymbol{p}+\boldsymbol{p}')/2$. For the matrix element Eq. (B4), the spatial part of the GCM kernel in Eq. (B3) is calculated to be

$$G^{\text{space}}(\boldsymbol{a},\boldsymbol{b}) = \frac{1}{(2\pi)^6\nu^3}\left(\frac{4+\zeta}{3\zeta}\right)^{3/2}\int d\boldsymbol{P}d\boldsymbol{k}'d\boldsymbol{q}'u(\boldsymbol{k}',\boldsymbol{q}';\boldsymbol{P}) \times \exp\left\{-\frac{1}{6\nu}\frac{\zeta+4}{\zeta+1}\boldsymbol{P}^2-\frac{1}{2\nu}\frac{\zeta+1}{\zeta}\left(\boldsymbol{q}'^2+\frac{1}{4}\boldsymbol{k}'^2\right) + i(\boldsymbol{a}-\boldsymbol{b})\cdot\left(\boldsymbol{q}'+\frac{\zeta}{\zeta+1}\boldsymbol{P}\right)+i\frac{1}{2}(\boldsymbol{a}+\boldsymbol{b})\cdot\boldsymbol{k}'\right\}. \quad \text{(B5)}$$

If we use Eq. (B5) in Eq. (B2), we can perform the integrals over $\boldsymbol{a}$ and $\boldsymbol{b}$ and obtain two delta functions. Thus we can perform the integrals over $\boldsymbol{k}'$ and $\boldsymbol{q}'$ and obtain a compact formula

$$V^{\text{space}}(\boldsymbol{q}_f,\boldsymbol{q}_i) = e^{-(3/32\nu)\boldsymbol{k}^2}\left(\frac{2}{3\pi\nu}\right)^{3/2}\int d\boldsymbol{P}e^{-(2/3\nu)\boldsymbol{P}^2} \times u\left(\boldsymbol{k},\frac{\zeta+4}{4(\zeta+1)}\boldsymbol{q}-\frac{\zeta}{\zeta+1}\boldsymbol{P};\boldsymbol{P}+\frac{3}{4}\boldsymbol{q}\right), \quad \text{(B6)}$$

where $\boldsymbol{k}=\boldsymbol{q}_f-\boldsymbol{q}_i$ and $\boldsymbol{q}=(\boldsymbol{q}_f+\boldsymbol{q}_i)/2$.

For a simple local Gaussian interaction, we find

$$u(\boldsymbol{k},\boldsymbol{q};\boldsymbol{P}) = \left(\frac{\pi}{\kappa}\right)^{3/2}\exp\left\{-\frac{\boldsymbol{k}^2}{4\kappa}\right\} \text{ for } u(r)=e^{-\kappa r^2},$$

$$u(\boldsymbol{k},\boldsymbol{q};\boldsymbol{P}) = \left(\frac{\pi}{\kappa}\right)^{3/2}\exp\left\{-\frac{1}{\kappa}\left(\boldsymbol{q}+\frac{1}{2}\frac{\zeta-1}{\zeta+1}\boldsymbol{P}\right)^2\right\} \text{ for } u(r)=e^{-\kappa r^2}P_r. \quad \text{(B7)}$$

Then the $\boldsymbol{P}$ integral is carried out easily and we obtain

$$V_d(\boldsymbol{q}_f,\boldsymbol{q}_i) = \left(\frac{\pi}{\kappa}\right)^{3/2}\exp\left\{-\frac{1}{4}\left(\frac{3}{8\nu}+\frac{1}{\kappa}\right)\boldsymbol{k}^2\right\} \text{ for } u(r)=e^{-\kappa r^2},$$

$$V_e(\boldsymbol{q}_f,\boldsymbol{q}_i) = \left(\frac{8\pi}{3}\frac{1}{\nu+\frac{8}{3}\kappa}\right)^{3/2}\exp\left\{-\frac{3}{32\nu}\boldsymbol{k}^2 - \frac{25}{24}\frac{1}{\nu+\frac{8}{3}\kappa}\boldsymbol{q}^2\right\} \text{ for } u(r)=e^{-\kappa r^2}P_r. \quad \text{(B8)}$$

If we further incorporate the spin-isospin factors, the full $V(\boldsymbol{q}_f,\boldsymbol{q}_i)$ is given by

$$V(\boldsymbol{q}_f,\boldsymbol{q}_i) = X_dV_d(\boldsymbol{q}_f,\boldsymbol{q}_i)+X_eV_e(\boldsymbol{q}_f,\boldsymbol{q}_i), \quad \text{(B9)}$$

with the spin-isospin factors defined by

$$\begin{Bmatrix} X_d \\ X_e \end{Bmatrix} = \langle\xi_\Lambda\chi_\alpha|\sum_{j=2}^{5}\begin{Bmatrix}\omega_{1j}^d \\ \omega_{1j}^e\end{Bmatrix}|\xi_\Lambda\chi_\alpha\rangle. \quad \text{(B10)}$$

Here χ_α is the spin-isospin wave function of the α-cluster. The partial wave decomposition of Eq. (B8) is given by

$$V_\ell^d(q_f,q_i;\kappa) = \left(\frac{\pi}{\kappa}\right)^{3/2}\exp\left\{-\frac{1}{4}\left(\frac{3}{8\nu}+\frac{1}{\kappa}\right)(q_f{}^2+q_i{}^2)\right\} \times i_\ell\left(\frac{1}{2}\left(\frac{3}{8\nu}+\frac{1}{\kappa}\right)q_fq_i\right),$$

$$V_\ell^e(q_f,q_i;\kappa) = \left(\frac{8\pi}{3}\frac{1}{\nu+\frac{8}{3}\kappa}\right)^{3/2}\exp\left\{-\frac{1}{4}\left(\frac{3}{8\nu}+\frac{25}{24}\frac{1}{\nu+\frac{8}{3}\kappa}\right)(q_f{}^2+q_i{}^2)\right\} i_\ell\left(\frac{1}{2}\left(\frac{3}{8\nu}-\frac{25}{24}\frac{1}{\nu+\frac{8}{3}\kappa}\right)q_fq_i\right), \quad \text{(B11)}$$

where $i_\ell(x)=i^\ell j_\ell(-ix)$ is the spherical Bessel function of imaginary argument.

[1] S. Saito, Suppl. Prog. Theor. Phys. **62**, 11 (1977).
[2] E. W. Schmid, Z. Phys. A **297**, 105 (1980).
[3] H. Kamada and S. Oryu, Prog. Theor. Phys. **76**, 1260 (1986).
[4] S. Oryu and H. Kamada, Nucl. Phys. A **493**, 91 (1989).
[5] S. Oryu, K. Samata, T. Suzuki, S. Nakamura, and H. Kamada, Few-Body Syst. **17**, 185 (1994).
[6] H. Horiuchi, Prog. Theor. Phys. **53**, 447 (1975).
[7] E. Hiyama, M. Kamimura, T. Motoba, T. Yamada, and Y. Yamamoto, Prog. Theor. Phys. **97**, 881 (1997).
[8] Y. Fujiwara, M. Kohno, and Y. Suzuki, Few-Body Syst. **34**, 237 (2004).
[9] E. M. Tursunov, D. Baye, and P. Descouvernont, Nucl. Phys. **A723**, 365 (2003).
[10] P. Descouvemont, C. Daniel, and D. Baye, Phys. Rev. C **67**, 044309 (2003).
[11] B. Buck, H. Friedrich, and C. Wheatley, Nucl. Phys. **A275**, 246 (1977).
[12] S. Ali and A. R. Bodmer, Nucl. Phys. **80**, 99 (1966).
[13] Y. Fujiwara, Y. Suzuki, and M. Kohno, Phys. Rev. C **69**, 037002 (brief report) (2004).
[14] Y. Fujiwara, H. Nemura, Y. Suzuki, K. Miyagawa, and M. Kohno, Prog. Theor. Phys. **107**, 745 (2002).
[15] Y. Fujiwara, Y. Suzuki, K. Miyagawa, M. Kohno, and H. Nemura, Prog. Theor. Phys. **107**, 993 (2002).
[16] Y. Fujiwara, K. Miyagawa, M. Kohno, Y. Suzuki, and H. Nemura, Phys. Rev. C **66**, 021001(R) (2002).
[17] Y. Fujiwara, C. Nakamoto, and Y. Suzuki, Phys. Rev. Lett. **76**, 2242 (1996); Phys. Rev. C **54**, 2180 (1996).
[18] Y. Fujiwara, T. Fujita, M. Kohno, C. Nakamoto, and Y. Suzuki, Phys. Rev. C **65**, 014002 (2002).
[19] Y. Fujiwara, K. Miyagawa, Y. Suzuki, M. Kohno, and H. Nemura, Nucl. Phys. **A721**, 983c (2003).
[20] R. Machleidt, Adv. Nucl. Phys. **19**, 189 (1989).
[21] A. Nogga, H. Kamada, and W. Glöckle, Phys. Rev. Lett. **85**, 944 (2000).
[22] Y. Fujiwara, K. Miyagawa, M. Kohno, and Y. Suzuki, Phys. Rev. C **70**, 024001 (2004).
[23] P. M. M. Maessen, Th. A. Rijken, and J. J. de Swart, Phys. Rev. C **40**, 2226 (1989).
[24] H. Bando, K. Ikeda, and T. Motoba, Prog. Theor. Phys. **69**, 918 (1983); **70**, 189 (1983).
[25] W. Brückner *et al.*, Phys. Lett. **55B**, 107 (1975).
[26] M. May *et al.*, Phys. Rev. Lett. **51**, 2085 (1983).
[27] D. H. Davis and J. Pniewski, Sov. J Contemp. Phys. **27**, 91 (1986).
[28] D. H. Davis, in *LAMPF Workshop on* (π,K) *Physics*, edited by B. F. Gibson, W. R. Gibbs, and M. B. Johnson, AIP Conf. Proc. No. 224 (AIP, New York, 1991), p. 38.
[29] H. Bando, T. Motoba, and J. Žofka, Int. J. Mod. Phys. A **5**, 4021 (1990).
[30] H. Akikawa *et al.*, Phys. Rev. Lett. **88**, 082501 (2002).
[31] H. Tamura *et al.*, in Proceedings of the Eighth International Conference on Hypernuclear and Strangeness Particle Physics, Jefferson Lab, Newport News, VA, 14–18 October 2003; Nucl. Phys. (to be published).
[32] E. Hiyama, M. Kamimura, T. Motoba, T. Yamada, and Y. Yamamoto, Phys. Rev. Lett. **85**, 270 (2000).
[33] Y. Yamamoto and Bando, Prog. Theor. Phys. **69**, 1312 (1983).
[34] I. N. Filikhin and A. Gal, Nucl. Phys. **A707**, 491 (2002).
[35] I. Kumagai-Fuse, S. Okabe, and Y. Akaishi, Phys. Lett. B **345**, 386 (1995).
[36] S. Oryu, H. Kamada, H. Sekine, H. Yamashita, and M. Nakazawa, Few-Body Syst. **28**, 103 (2000).
[37] E. Cravo, A. C. Fonseca, and Y. Koike, Phys. Rev. C **66**, 014001 (2002).
[38] Y. Fukushima and M. Kamimura, J. Phys. Soc. Jpn. Suppl. **44**, 225 (1978).
[39] E. Uegaki, S. Okabe, Y. Abe, and H. Tanaka, Prog. Theor. Phys. **57**, 1262 (1977); **62**, 1621 (1979).
[40] P. Descouvemont and D. Baye, Phys. Rev. C **36**, 54 (1987).
[41] Y. Fujiwara, M. Kohno, K. Miyagawa, Y. Suzuki, and J.-M. Sparenberg, Phys. Rev. C , No. 3 (2004); nucl-th/0405056.
[42] J.-M. Sparenberg and D. Baye, Phys. Rev. C **55**, 2175 (1997).
[43] W. Glöckle, *The Quantum Mechanical Few-Body Problem*, Texts and Monographs in Physics (Springer, Berlin, 1983).
[44] K. Miyagawa and W. Glöckle, Phys. Rev. C **48**, 2576 (1993).
[45] D. R. Thompson, M. LeMere, and Y. C. Tang, Nucl. Phys. **A286**, 53 (1977).
[46] Y. Fujiwara, M. Kohno, C. Nakamoto, and Y. Suzuki, Phys. Rev. C **64**, 054001 (2001).
[47] R. H. Dalitz, R. C. Herndon, and Y. C. Tang, Nucl. Phys. **B47**, 109 (1972).
[48] H. Bando and I. Shimodaya, Prog. Theor. Phys. **63**, 1812 (1980).
[49] H. Nemura, Y. Akaishi, and Y. Suzuki, Phys. Rev. Lett. **89**, 142504 (2002).
[50] M. Kohno, Y. Fujiwara, and Y. Akaishi, Phys. Rev. C **68**, 034302 (2003).
[51] Y. Fujiwara, M. Kohno, C. Nakamoto, and Y. Suzuki, Prog. Theor. Phys. **104**, 1025 (2000).
[52] A. B. Volkov, Nucl. Phys. **74**, 33 (1965).
[53] H. Matsumura and Y. Suzuki, Nucl. Phys. **A739**, 238 (2004).
[54] C. M. Vincent and S. C. Phatak, Phys. Rev. C **10**, 391 (1974).
[55] D. R. Lehman, A. Eskandarian, B. F. Gibson, and L. C. Maximon, Phys. Rev. C **29**, 1450 (1984).
[56] W. Glöckle, G. Hasberg, and A. R. Neghabian, Z. Phys. A **305**, 217 (1982).
[57] See ARPACK homepage, http://www.caam.rice.edu/software/ARPACK/
[58] J. A. Koepke, R. E. Brown, Y. C. Tang, and D. R. Thompson, Phys. Rev. C **9**, 823 (1974).
[59] Y. Fujiwara, H. Horiuchi, K. Ikeda, M. Kamimura, K. Kato, Y. Suzuki, and E. Uegaki, Suppl. Prog. Theor. Phys. **68**, 29 (1980).
[60] Y. Yamamoto, T. Motoba, H. Himeno, K. Ikeda, and S. Nagata, Prog. Theor. Phys. Suppl. **117**, 361 (1994).
[61] H. Takahashi *et al.*, (KEK-PS E373 collaboration), Phys. Rev. Lett. **87**, 212502 (2001).
[62] Y. Fujiwara, M. Kohno, T. Fujita, C. Nakamoto, and Y. Suzuki, Prog. Theor. Phys. **103**, 755 (2000).
[63] C. Nakamoto, Y. Suzuki, and Y. Fujiwara, Prog. Theor. Phys. **94**, 65 (1995).